FE modeling of contemporary tectonic stress in the India-Eurasia collision zone

FE modeling of contemporary tectonic stress in the India- Eurasia collision zone

Deepak Chamlagain and Daigoro Hayashi

Simulation Tectonics Laboratory
Department of Physics and Earth Sciences
University of the Ryukyus, Nishihara, Okinawa, 903-0213, Japan

Abstract

An understanding of orientation of contemporary maximum horizontal compressive stress (σ_{Hmax}) is important to many aspects of earth sciences, e.g. seismicity, neotectonics, and plate driving mechanisms. Comparison of recent stress observations and the results of stress modeling provide a powerful approach to refine our understanding of geodynamics processes. This is especially important for complex area like Himalayan-Tibet orogen, a continental collision zone between the Indian and Eurasian Plates. The frequently occurring earthquakes and other tectonic stress indicator have provided vast set of database on maximum horizontal compressive stress (σ_{Hmax}) that can be useful to study contemporary stress sources, plate kinematics and ongoing geodynamics. In this contribution, taking advantage of elastic plane stress finite element modeling (FEM), and observed data on σ_{Hmax}, several models are presented to reproduce stress field. Simulated models show that the convergence normal to the orogen is essential to reproduce observed σ_{Hmax}, which in turn controls the magnitude and orientation of σ_{Hmax}. The kinematics equivalent to east-west tectonic escape did not reproduce the observed stress field. Therefore, the best-fit model of present day stress field is obtained only in three domains model with southeastward tectonic escape of the Tibetan crust rather than eastward extrusion. There is, however, significant increase in σ_{Hmax} magnitude with increasing crustal depth because of stress amplification. Incorporation of suture zones in the model did not change orientation of σ_{Hmax} significantly. Considering these facts, 'continuum tectonic model' is more preferable than the 'block tectonic model' for the active deformation of the Tibetan Plateau. Contemporary stress field deduced from several tectonic stress markers reconciles with the predicted one giving insights on their sources and ongoing plate kinematics of the continental collision zone between Indian and Eurasian Plates.

Received: January 15, 2008

1. Introduction

The collision zone between Indian and Eurasian Plates is characterized by unique landscapes on the earth surface: first, the world famous mountain ranges, the Himalaya, comprising most of the highest peaks of the world and second a thick Tibetan Plateau up to five kilometers elevation, just north of the Himalaya. The Himalaya is the most inspiring example of an active collisional orogen on the globe. The entire 2400 km long mountain range from Kashmir in the west to Arunachal in the east is the outcome of its unique geodynamics, tectonics, crustal shortening and thickening and intense denudation driven by both tectonics and climate. Catastrophic earthquakes that occur along the several active thrust faults, which are accumulating elastic stress/strain in the interseismic periods, reveal its dynamic nature. Several geodetic studies (Bilham et al. 1997; Larson et al. 1999; Jouanne et al. 2004) have also precisely determined the internal deformation and elastic stress and strain accumulation due to ongoing underthrusting of the Indian Plate beneath the Himalaya. Similarly, microseismic data (Pandey et al., 1995) have clearly shown the earthquake swarms along the topographic front of the Higher Himalaya and their location are particularly controlled by fault geometry and its behavior. On the other hand, north of the Himalaya, large Tibetan Plateau is characterized by almost extensional tectonics. The extensional features comprise of north trending normal faults, associated grabens, and E-W trending strike-slip faults. Furthermore, Tibetan Plateau is seismically active zone, and fault plane solutions data indicate that, except for low angle thrusting to the south below the Himalaya, active tectonics of the Tibet is dominated by east-west extension, with focal depths for most events about 5-10 km (Molnar and Tapponnier, 1978). Most of the focal mechanism data show a large component of normal faulting but some indicate a strike-slip motion.

An understanding of orientation of contemporary maximum horizontal compressive stress (σ_{Hmax}) is important to many aspects of earth sciences, e.g. seismicity, neotectonics, and plate driving mechanisms. Comparison of recent stress observations and the results of stress modeling provide a powerful approach to refine our understanding of geodynamics processes. This is especially important for complex area like Himalayan-Tibet orogen, a continental collision zone between Indian and Eurasian Plates, because a complex and enigmatic geodynamic processes are active in the region and the state of lithospheric stress is governed by many distinct factors; such as topography, buoyancy forces, and rheological stratification. The results of previous modelings (Cloetingh and Wortel, 1986; Kong and Bird, 1996; Bada et al., 1998; Flesch et al., 2001; Reynolds et al., 2002; Dyksterhius et al., 2005; Petit and Fournier, 2005) have clearly shown that the plate tectonic processes can be simulated using finite element method. In addition, our knowledge on contemporary stress (Zoback et al., 1989; Zoback et al., 1992; Zhonghuai et al., 1992; Reinecker et al., 2005) and the present-day crustal deformation (Molnar and

Tapponier, 1975; Rothery and Drury, 1984; Bilham et al., 1997; Larson et al., 1999; Wang et al., 2001; Chen et al., 2004) in the Himalayan-Tibet orogen has greatly been improved during last two decades. This enables construction of the simple but geotectonically reasonable models to analyze how the collision zone stresses are influenced by tectonic discontinuities, regional boundary conditions and plate kinematics. Therefore, in this research, it is aimed to study relative importance of different boundary conditions to explain nature and sources of observed stress pattern in the India-Eurasia collision zone by applying two-dimensional finite element modeling method (Hayashi, 2007) giving emphasis on geodynamics, tectonic boundary conditions and origin of stress field. Overall validity of the models can be assessed by comparing their predictions with the huge database of the World Stress Map (WSM) (Reinecker et al., 2005). Further, this kind of model study is important to shade light on the debate between supporters of "continuum tectonics" and "block tectonics" model for the active deformation of the India-Eurasia collision zone.

2. Geodynamic Setting of the Himalaya-Tibet Orogen

The entire Himalayan orogen is the major zone of the active deformation, which has absorbed the indentation of the Indian Plate into the Eurasian Plate. The collision has started about 50 Ma ago and produced a combination of the crustal thickening and lateral tectonic escape (Fig. 1.), which has given rise to the highest topographic features on the earth (Molnar and Tapponier, 1975; Harrison et al., 1992). Before the advent of theory of plate tectonics, Himalaya was considered as having been formed due to continent-continent collision between Indian and Eurasian Plates (Gansser, 1964). Powell and Conaghan (1973) suggested that the simple continent-continent collision model does not produce present-day

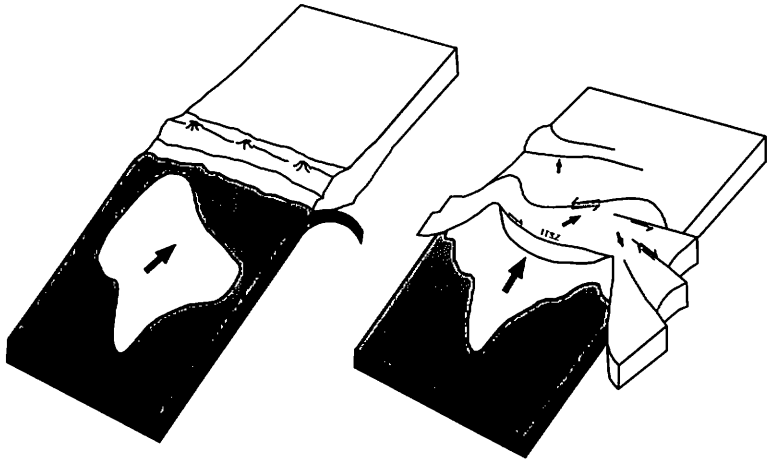

Fig.1. Cartoon showing indentation of Indian Plate into Eurasian Plate. Note that indentation caused large crustal thickening and lateral escape in the collision zone (after Avouac, 2003)

Himalaya. They, alternatively, proposed an evolutionary model invoking two phases orogeny. First, active Mesozoic-early Tertiary subduction zones along the present-day Indus-Tsangpo suture zone. This phase was ended in Eocene when collision occurred between two plates. Second phase is characterized by the formation of the intracontinental thrusts from Miocene to the present within the Indian Plate in which Indian plate is underthrusting from during middle Tertiary to the present. After the plate tectonics theory, vast amounts of data were accumulated and several plate tectonic models have been proposed. These models commonly emphasized that (a) early convergence between India and Eurasia took place along the Indus-Tsangpo suture (b) the suture closed during the Late Cretaceous-Eocene (c) after the closure of the Neo-Tethys, Himalaya was formed due to collision. Consequently, collision produced a combination of crustal shortening in the Himalaya and crustal thickening in the elevated Tibet, which later extruded probably due to gravitational collapse ~ 14 Ma ago. At present Indian Plate is converging to the Eurasia at the rate of 5 $cmyr^{-1}$ (Patriat and Achache, 1984). Part of this convergence (2 $cmyr^{-1}$) is still being absorbed by a horizontal shear and crustal shortening in the Himalaya as shown by GPS data (Bilham et al., 1997; Jouanne et al., 2004) and Quaternary fault slip rates (Lave and Avouac, 2000) in the Himalaya. The processes of crustal shortening are still active in the Himalaya as manifested by large earthquakes (Mw>8) e.g. Bihar Nepal earthquake (1934), Kangara earthquake (1905) or the Pakistan earthquake (2005). Apart from these, crustal shortening is being occurred due to southward propagation of the thrusts. However, to the north of the Himalaya, entire Tibetan Plateau is known for the extensional tectonics characterized by movement along the E-W trending strike-slip faulting and N-S striking normal faulting and associated grabens. The GPS data have revealed a clockwise rotation of GPS vectors around the eastern Himalayan syntaxis leading a movement in southeast direction with decreasing velocity rates towards the South China Sea (Wang et al., 2001). The overall kinematics derived from the GPS support the "Block tectonic model" (Thatcher, 2007; Meade, 2007). On the other hand, there are several crustal scale models (e.g., Flesch et al., 2001; Chen et al., 2004) in favor of "Continuum tectonic model".

3. Geotectonic setting

3.1. Himalayan fold-and-thrust belt

The regional structural geology of the fold-and-thrust belt of Nepal Himalaya to the south of South Tibetan Detachment System (STDS) (Burchfiel et al., 1992) is controlled mainly by three major thrust systems, e.g. from north to south the MCT, MBT and MFT (Fig. 2). These thrust faults with the N-S transport direction are generally inferred to be splay thrusts of the MHT, which marks the underthrusting of the Indian Plate. Most of the cross-sections across the Himalaya suggest a mid-crustal ramp, below a large

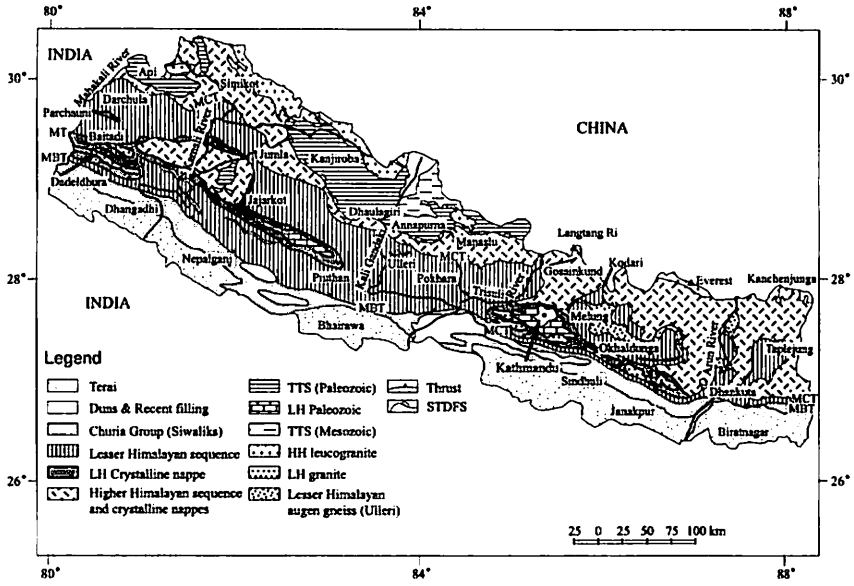

Fig.2. Geological map of Nepal (modified after Upreti and Le Fort, 1999). LH: Lesser Himalaya, HH: Higher Himalaya, TTS: Tibetan-Tethys sequence, MBT: Main Boundary Thrust, MCT: Main Central Thrust, MFT: Main Frontal Thrust, STDS: South Tibetan Detachment System.

antiformal structure of the Lesser Himalaya and north of synformal structure (Schelling and Arita, 1991; DeCelles et al., 2001). Geological, geophysical and structural data have inferred the lateral variation in geometry of the MHT (e.g. Zhao et al., 1993; Pandey et al., 1995).

The MFT system consists of two or three thrust sheets composed entirely of Siwalik rocks, from bottom to top mudstone, multi-storied sandstone and conglomerate (Table 1). These sedimentary foreland basin deposits form an archive of the final stage of the Himalayan upheaval and record the most recent tectonic events in the entire history of Himalayan evolution since ~ 14 Ma. In general, this belt exhibits fault bend fold structure throughout the Nepal Himalaya. Minor structures include normal faults with centimeter to meters displacements. The northernmost thrust sheet of the MFT is truncated by the Lesser Himalayan sequence and overlain by unmetamorphosed to weakly metamorphosed rocks of the Lesser Himalaya, where the Lesser Himalayan rock package is thrust over the Siwalik Group along MBT. In western Nepal crystalline thrust sheets are frequently observed within the Lesser Himalaya, e.g. Dadeldhura crystalline thrust sheet (Hayashi et al., 1984). The Lesser Himalayan zone generally forms a duplex above the mid crustal ramp (Schelling and Arita, 1991; DeCelles et al., 2001). The MCT system overlies the Lesser Himalayan MBT system and was formed in ca. 24 Ma. This MCT system consists of high-grade rocks, e.g. kyanite-sillimanite gneiss, schist and quartzite and is mostly characterized by ductile deformation.

Table.1. Major tectonic division of the Himalaya.

Geologic unit	Main rock types	Age
1. Terai zone (Gangetic Plain)	Alluvium: coarse gravels in the north near the foot of the mountains, gradually becoming finer southward. Foreland basin deposits.	Recent
Main Frontal Thrust		
2. Siwalik	Sandstone, mudstone, shale, and conglomerate. Mollase deposits of the Himalaya.	Mid-Miocene to Pleistocene
Main Boundary Thrust		
3. Lesser Himalaya	Schist, phyllite, gneiss, quartzite, granite and limestone.	Precambrian and Paleozoic ocassionally Cenozoic
Main Central Thrust		
4. Higher Himalayan Sequence	High grade gneiss, schist and marbles.	Precambrian
South Tibetan Detachment Fault System		
5. Tibetan-Tethys Sequence	Tethyan sediments (limestone, shale, sandstone etc.).	Precambrian and Cambrian to Cretaceous

3.2. Tibetan Plateau and adjacent areas

High-elevation Tibetan Plateau, north of the Himalaya, is important to understand geodynamics of the continental collision zone. Tibetan Plateau is a contiguous region of high (>4.5 km) elevation that extends between the latitudes 72°E and 990E. The Altyn Tagh Fault bound it to the north and Indus-Tsangpo suture zone to the south against the Himalaya (Fig. 3). The entire plateau is characterized by the low relief. However, Plateau has very steep slopes at the periphery sometime it exceeds 6 km. Overall local topographic relief decreases systematically northward across the Plateau.

The entire Plateau can be divided into three large crustal blocks: the Lhasa, Qiangtang, and Songpan-Ganzi terranes (Matte et al., 1996) (Fig. 3). The Songpan-Ganzi terrane is exposed between the Kunlun suture zone on the north and on the south by Jinsha suture. It is basically composed of thick turbidites that were deposited during Triassic in a remnant ocean basins west of the Qinling-Dabie orogenic belt. In the eastern part, this block has experienced thin-skinned thrusting and shortening of several tens of kilometers during early Tertiary. To the south of the Songpan-Ganzi blocks, Qiangtang block is cropped out between the Jinsha suture to the north and the Banggong suture zone to the south (Fig. 3). This terrane consists of metamorphic rocks overlain in structural contact by upper Paleozoic and Mesozoic strata. The metamorphic rocks comprise of

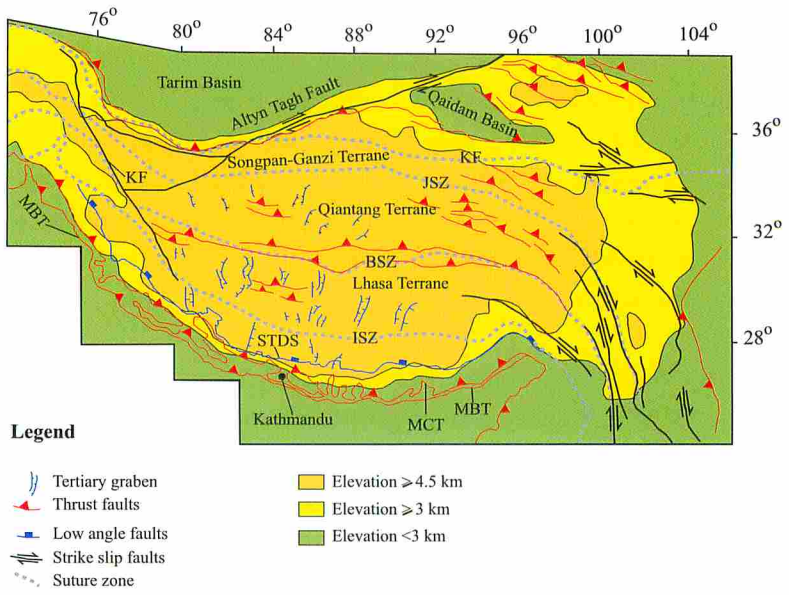

Fig.3. Regional geotectonic map of the Himalaya-Tibet orogen showing major suture zones, terraines and faults. BNS: Bangong Nujiang Suture; ITSZ: Indus-Tsangpo Suture Zone; JS: Jinsha Suture (modified after DeCelles, et al., 2002)

metasedimentary and mafic schists that enclose partially metamorphosed metabasites and minor ultramafic rocks. The Lhasa terrane demarcated by Banggong suture to north and Indus Tsangpo suture zone to the south is composed of medium-to high-grade metasedimentary rocks of late Precambrian-early Paleozoic age overlain by Orodovician and Carboniferous to Cretaceous sedimentary rocks. The extensive Cretaceous-Eocene Gangedese batholith belt intrudes the southern part.

Structurally, Tibetan Plateau is characterized by two sets of normal faults and several strike-slip faults with both right and left lateral movement (Tapponier et al., 2001). The normal fault systems include northwest-southeast to east-west striking South Tibetan Detachment (STD) system, north-south striking normal fault and associated grabens. These grabens are mainly distributed along the crest of the Himalaya, southern and central Tibet (Fig. 3) and are results of the Cenozoic extensional tectonic phase, which has affected whole Tibet and northernmost part of the Himalaya. The major grabens of the Himalaya are, from west to east, Burang graben, the Thakkhola graben, Gyirong graben, Kungo graben, Pum Qu graben and Yadong graben. In the Himalaya, all the grabens are limited south of the ITSZ except Yadong graben, which extends up to Gulu rift. The onset of normal faulting, which corresponds initiation of graben, was estimated to commence in the Southern Tibet and Himalaya 14 Ma ago (Coleman and Hodges, 1995) about 4 Ma ago (Yin et al., 1999) in central Tibet. However, Blisnuik et al. (2001) reported a minimum age of approximately 13.5 Ma for the onset of graben formation in central Tibet, based on mineralization ages on fault plane. The graben spacing in the Himalaya and Tibet

decreases systematically from south to north. In the Himalaya, it is 191±67 km. In south Tibet, it is 146±34 km. Farther north in central Tibet, it is 101±31 km. The widely spaced grabens in the Himalaya and Tibet may have been related to the presence of a relatively light crust and a strong mantle lithosphere throughout Tibet (Yin, 2000). Systematic decrease in graben spacing can also be attributed to the northward decrease in crustal thickness. Numerical study has indicated that these grabens are result of gravitational collapse driven by excess gravitational potential energy of elevated plateau rather than the asthenospheric upwelling beneath the Himalaya-Tibet orogen (Chamlagain and Hayashi, 2006).

Several strike-slip faults are located on the Tibetan plateau, including right-lateral Altyn Tagh fault, Kunlun fault, right-lateral Karakoram fault, Jiali fault, Red River fault. The Altyn Tagh fault marks the northern boundary of the Tibetan Plateau and has accommodated very large amount (280-550 km) of slip (Wang et al., 2001). The left and right-lateral strike- slip faults have translated eastern Tibet towards east giving rise to large-scale crustal extrusion. It is considered that right-lateral Karakoram fault in the western part of the Plateau transfer the slip between the Himalayan fold-and-thrust belt and the Pamir Range.

In addition to widely distributed strike-slip and normal faulting, there are number of moderate-sized earthquakes at depth of 13-70 km showing strike-slip and extensional focal mechanism (Chen and Kao, 1996). The direction of extension is approximately east-west, at nearly a right angle to the direction of compression in the Himalaya.

4. Seismicity and Neotectonics of the Himalaya-Tibet Orogen

The Himalaya-Tibet orogen is the one of most seismically active region on the globe (Fig. 4). Numbers of small, medium and large magnitude earthquake has been recorded throughout the Himalaya. Owing to the short instrumental record of the seismic events, the distribution of seismicity throughout the Himalaya appears nonuniform although a major trend has been recognized. The general trend consists of a narrow belt of predominantly moderate sized earthquakes beneath the Lesser Himalaya just south of the Higher Himalayan front (Ni and Barazangi, 1984) where all available fault-plane solutions indicate thrusting. This belt can easily be traced along the entire Himalaya. Seeber et al. (1981) believe that a decollement surface underlies the entire Himalaya, which represents the upper surface of the underthrusting Indian Plate. They also argued the presence of Basement thrust (BT) where northerly, and relatively dipping MCT merges with the shallow dipping detachment surface at depth. They further claimed that most of the moderate-sized earthquake events occur either along the BT or along the downdip projection of the MCT. The great Himalayan earthquakes, however, occur along the basal decollement beneath the Siwalik and Lesser Himalaya. The focal depth for the Himalayan

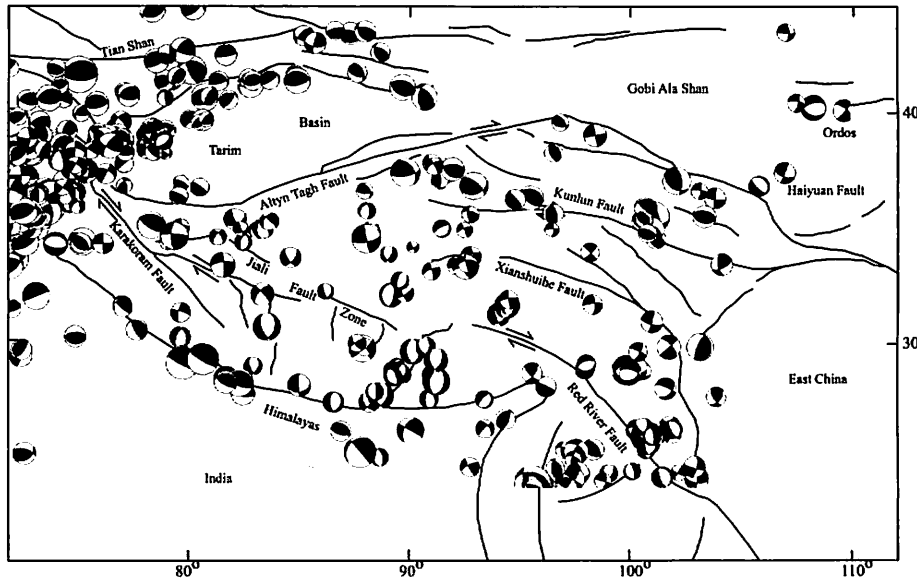

Fig.4. Seismicity map of the Himalaya-Tibet region. Structural data from Thatcher (2007) and CMT focal mechanism solution data from http://discoverourearth.org/webmap

earthquake varies from 10-20 km. In both the eastern and western syntaxes, earthquakes have shallow focal depths in the south, but become deeper towards the north.

In Tibet, earthquakes are distributed mainly along the N-S striking structural belts, along NE and NW strike-slip fractures (Fig. 4) and in south-central Tibet along E-W striking strike-slip faults, with large numbers of faults in the western and eastern syntaxes. In the eastern and western syntaxes, the frequency of deep focus earthquakes is very high. In the western syntaxis, some earthquakes have occurred at more than 25 km depth, but are distributed vertically with no evidence of underthrusting. In southern Tibet and in most areas of south-central Tibet, focal depths are about 10-35 km. In southern and south-central Tibet, the major earthquakes have a shallow focus. In the interior of the Tibetan Plateau, earthquakes deeper than 70 km are mainly distributed along Xigaze-Anduo and Gongbujingda-Dingqing zones, and some along the MCT, besides those within the west Kunlun Mountains belt. Although there are many E-W striking structures, especially thrusts and overriding structures, at least at the present time, the N-S, NE-, and NW-striking structures control the seismic activity, while the E-W striking structures have not given rise to either deep or shallow earthquakes in Himalayan-Tibet region.

Based on an analysis of the focal mechanisms two types of mechanism are dominant in southern Tibet: thrusts, located mainly in the High Himalaya indicating N-S compression, and normal faults indicating E-W-extension, in most other areas of southern Tibet (Fig. 4). NE- and NW-striking strike-slip faults are distributed mainly in the western and eastern syntaxes, and in the central part of the Tibetan Plateau. Earthquakes also occur

along E-W striking structural belts such as the Jiali Fault, the Bangong-Nujiang Suture Zone, the Jinsha Suture, and the Kunlun Fault Zone. In southern Tibet, the mechanisms show compressive stress, especially in the arcuate Himalayan structural belt; although this area is affected by, N-S striking faults. The eastern syntaxis is dominated by strike-slip faults, but there are a large number of thrust faults in the western syntaxis, especially in the northern part of the area. This reflects the N-S compression and overthrusting which are still active in this area. Earthquakes along the Xigaze-Anduo zone show normal mechanisms; the western syntaxis shows both shear-slip and thrust types of mechanism; in the southern part of the eastern syntaxis, earthquakes are mainly of thrust type (Chen et al., 1981; Molnar and Chen, 1983). At the southeast boundary of the Tibetan plateau, there are no obvious sinistral strike-slip mechanisms, while mechanisms are largely dextral.

In central Tibet, earthquakes are distributed mainly along the Bengcuo-Jiali Seismic Belt. Many earthquakes have occurred along the Bangong-Nujiang Suture Zone, but very strong earthquakes have occurred on the Bengcuo-Jiali NW-SE-striking dextral strike-slip fault. Toward north, there is another seismic belt, named the Yanshiping-Dingqing-Changdu Seismic Belt, consisting of a few short and discontinuous faults with a NW-SE strike. To the east is the Xianshuihe Seismic Belt, which is a sinistral strike-slip fault. In these belts, a few earthquakes reflect dextral strike-slip along the Bengcuo-Jiali Belt, and sinistral strike-slip along the Yanshiping-Changdu Belt, which is consistent with the active characteristics of the faulting. However, in the Xianshuihe Fault Belt, earthquakes show two different types of mechanism: sinistral strike-slip and extension; even at the same place earthquakes show different mechanisms (Molnar and Chen, 1983).

5. State of present day stress field and crustal deformation pattern in the Himalaya-Tibet orogen: constrains for modeling

The Himalaya-Tibet orogen and surrounding regions demonstrate very complex contemporary stress field pattern that reflects present-day geodynamics of the region. Because the Indian plate is underthrusting below the Eurasian plate and subsequently thrust faults are propagating to the foreland side of the Himalaya indicating southernmost front as a most active zone. This is clearly manifested by focal mechanism solution of a moderate to large earthquakes. Most of the events are of thrust type. However, there are some events along the transverse fault indicating strike-slip motion. On the other hand, the entire Tibetan Plateau generally characterized by extensional tectonics. It is inferred that the elevated landform is tectonically escaping towards east-south-east along the major strike-slip faults. The seismicity in and around the Plateau has revealed mainly strike-slip and few normal faulting events. Using P-wave first motion polarity readings and P and T axes of the focal mechanism solution of the 5054 small

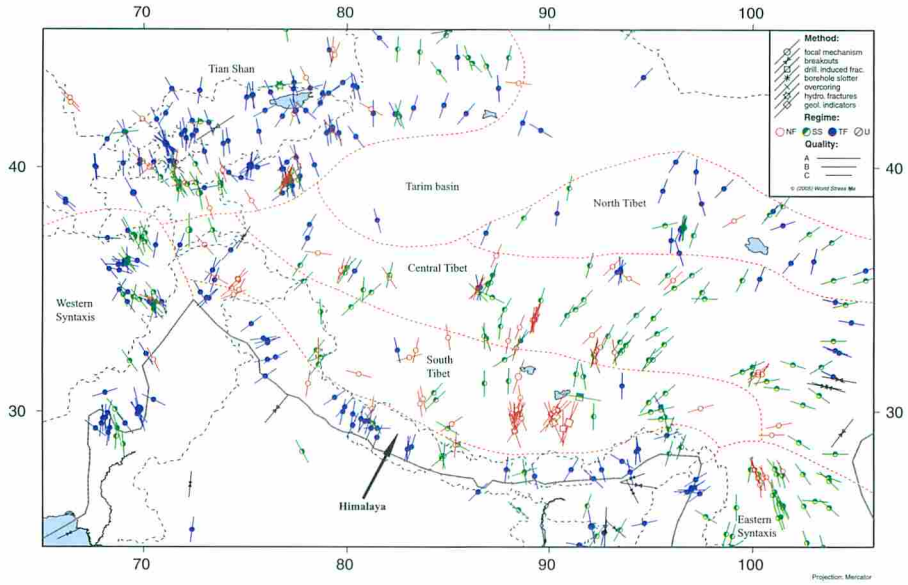

Fig.5. Maximum horizontal compressive stress (σ_{Hmax}) observed in and around the modeled area (after Reinecker et al., 2005).

earthquakes (1 ML<5), Zhonghuai et al. (1992) predicted mean principal stress axes for China and surrounding regions. They inferred that the P and T axes are dominantly horizontal, and the intermediate (B axes) are vertical indicating deformation primarily takes place through strike-slip faulting in the Tibetan Plateau and surrounding areas except Himalayan region. These data suggest that the principal stress axes have a relatively uniform radial pattern. The maximum horizontal compressive stress trajectories radiate from the Tibetan Plateau to the northern, eastern, and southeastern part of the Chinese mainland. However, the minimum horizontal compressive stress direction arc convex outward from the Tibetan Plateau. In the western part of the Tibetan Plateau near the Tian Shan, maximum horizontal stress axes are northwesterly oriented and minimum stress axes are vertical indicating thrust faulting regime. For the Himalayan region their data are limited and sparse however, eastern syntaxis shows sharp bending of stress trajectories towards southeast direction.

Recently, WSM project (Reinecker et al., 2005) has presented an extensive data set on stress field in Himalayan-Tibet region (Fig. 5). Different types of stress indicators are used to determine the tectonic stress orientation, which are grouped into four categories: earthquake focal mechanisms, well bore breakouts and drilling-induced fractures, in-situ stress measurements (overcoring, hydraulic fracturing, borehole slotter) and young geologic data (from fault-slip analysis and volcanic vent alignments). The stress map produced by WSM exhibits a complex pattern of present-day maximum horizontal stress (σ_{Hmax}) directions. Despite the heterogeneous distribution and quality variation of the

available data, the entire Himalayan-Tibet orogen can be divided into six stress provinces, e.g. Himalaya, Tibetan Plateau (southern Tibet, central Tibet and northern Tibet), Tian Shan and Pamir Plateau, Tarim basin (including lowland areas), western syntaxis and eastern syntaxis, where the stress direction of σ_{Hmax} reveal a good consistency (Fig. 5).

Stress data for the Himalaya is mostly derived from the earthquake focal mechanims, few are taken from direct stress measurements using breakouts. This region is mostly characterized by thrust faulting with very few strike-slip events. The direction of σ_{Hmax} is almost parallel to the direction of plate convergence at least in the central sector of the Himalaya. The trend of σ_{Hmax} is almost north in the central part. However, in the eastern part, this direction is towards northwest but in the western Himalaya, this trend changes towards northeast. It seems that trajectory of σ_{Hmax} converges towards north. The stress directions given by strike-slip events are not uniform and are mostly located south of the Himalaya. The direction of the σ_{Hmax} gradually changes from its northwest direction towards northeast in the eastern syntaxis and finally rotates to southeast direction. In contrast, in the western syntaxis its direction gradually deviates to northwest from its northeast direction. These observations clearly show gradual change in direction of σ_{Hmax} in the Himalaya. There are few strike-slip events related transcurrent faults. The overall stress patterns show that σ_{Hmax} is in direction of plate convergence in the central sector of the Himalaya and radiate outward in syntxes, which is consistent with the structural features of the region.

Tibetan Plateau has revealed a very complex and interesting pattern of σ_{Hmax} direction. It can be divided into three sub-stress provinces e.g., south Tibet, central Tibet, and north Tibet because each region is characterized by distinct earthquake focal mechanism, stress regime and active deformation characterized by GPS data. The stress data for the Tibetan Plateau also consists of earthquake focal mechanisms, well bore breakouts and drilling-induced fractures, in-situ stress measurements (overcoring, hydraulic fracturing, borehole slotter) and young geologic data (from fault-slip analysis and volcanic vent alignments). Southern Tibet is dominantly characterized by the normal faulting with few strike-slip faulting. Immediately after the Himalaya, σ_{Hmax} is oriented towards northeast direction in the southwestern region of the southern Tibet. This trend gradually changes towards eastern and central Tibetan Plateau. In the central southern Tibetan Plateau, σ_{Hmax} gradually rotates towards east. Central part of Tibetan Plateau is largely dominated by strike-slip events and σ_{Hmax} mainly oriented in the northeast direction but is changed towards east in the east central Tibet. In the northern Tibetan Plateau, σ_{Hmax} direction derived from the focal mechanism data and is extensively oriented towards north to slightly north-east direction. These are largely of thrust type except for the north China where events are strike-slip type and σ_{Hmax} is almost oriented in north-east-east direction.

Interestingly, Pamir Plateau shows the quite uniform northwest orientation of σ_{Hmax} and is characterized by both thrust and strike-slip tectonics. Although σ_{Hmax} orientation in

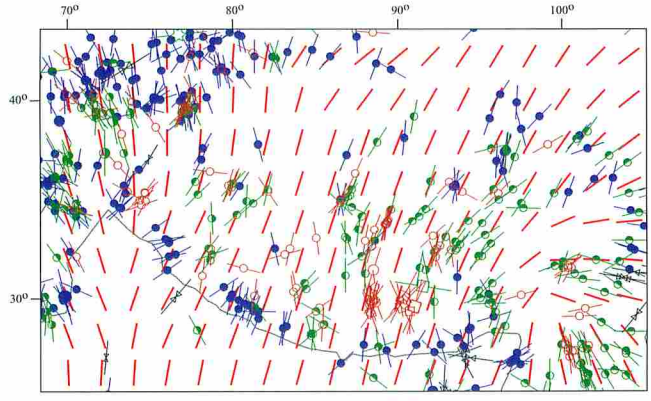

Fig.6. Smoothed directions of observed maximum horizontal compressive stress (sHmax) for the available data in Himalaya-Tibet orogen (after Reinecker et al., 2005).

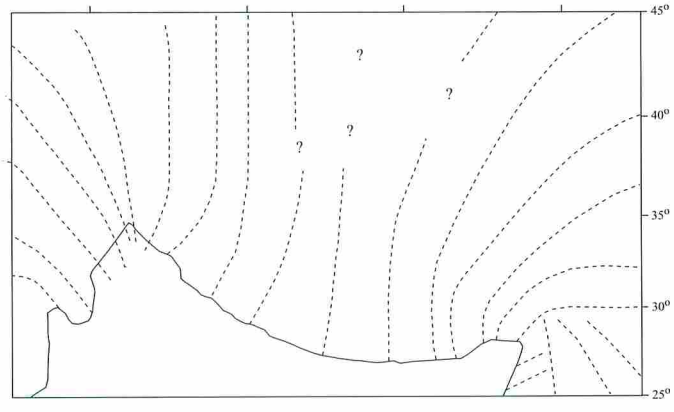

Fig.7. sHmax trajectory of observed data in India-Eurasia collison zone.

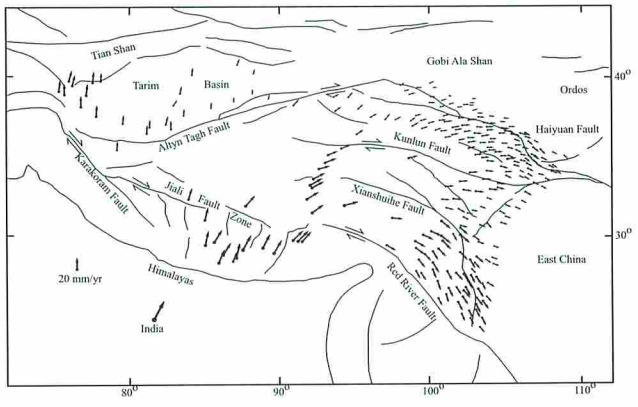

Fig.8. Himalaya-Tibet and surrounding regions, with GPS velocity vectors relative to stable Eurasia (Thatcher, 2007). Gray lines show active faults.

the Tian Shan region is almost similar to Pamir Plateau, stress regime is dominantly thrust type indicating active compressional tectonics. The σ_{Hmax} shows the counterclockwise rotation in the western syntaxis and adjoining region. There are few earthquake events in the Tarim basin and lowland area by which it is difficult to infer general trend of the σ_{Hmax}. This suggests that this area behaves like a rigid undeformed tectonic block. Overall Himalaya-Tibet orogen shows an interesting feature of σ_{Hmax} orientation, because σ_{Hmax} is almost north south in the central sector and it gradually rotates clockwise direction in the eastern Tibet and eastern Himalayan syntaxix. In contrast, in western Tibet, Pamir Plateau and western syntaxis, σ_{Hmax} rotates counterclockwise direction. Fig. 6 shows smoothed direction of observed σ_{Hmax} using interpolating and extrapolating technique of Muller et al. (2003). This technique provides fidelity and smoothness of the generalized map obtained from the original data. Figure 7 displays tentative σ_{Hmax} trajectory drawn from observed data for the entire region.

Recently, Global Positioning System (GPS) has provided clear pattern of deformation in the Himalayan-Tibet region (Fig. 8) (Bilham et al., 1997; Larson et al., 1999; Wang et al., 2001; Jouanne et al., 2004). GPS data have shown that much of the actively deforming part of Himalaya-Tibet lies within China, including the Tibetan Plateau, and parts of the Himalaya, Tian Shan, and Pamir mountain range. Stations located on the northern Ganges plains, south of the Himalaya, show northward movement at a rate of 36 to 38 $mmyr^{-1}$ with respect to stable Eurasia. The maximum velocity ($\sim$38 $mmyr^{-1}$) of sites in the northern Ganges plain approximates the rate of convergence between the Indian and Eurasian plates. This estimate is also similar to that (36 3.5 $mmyr^{-1}$) inferred from Quaternary fault slip. In the Tian Shan of northwest China (Fig. 8), widespread active faulting and folding, recent uplift, and high seismicity attest to rapid crustal shortening. Across its western part, velocity ranges from of 20 to 22 $mmyr^{-1}$ towards south. The total shortening rate between longitudes 81° E and 85° E is only 4.7 1.5 $mmyr^{-1}$. The movement direction is almost north to north eastward. The North China region including the Ordos block and the North China Plain show east-southeastward movement at rates of 2 to 8 $mmyr^{-1}$ to the direction of south-southeast. Major active faults in the North China region trend north-northeast. The oblique intersections with the south-southeastward movement probably produce right-lateral strike-slip components along those faults, which cause major earthquakes with the same prominent component. Although GPS observation net in the Tibetan plateau is not dense, it can be seen that large displacement vectors toward the north or north-north-east directions distributed along the Himalayan belt and the southern Tibetan plateau. The medium displacement vectors in the central plateau are slightly less than those along the Himalayas, and change the orientations into the northeast direction. Large movement vectors mixing with some small ones in the north-south, north-north-west to south-south-east and north-north-west-south-south-east directions lie complicatedly in the regions northwest of

Kunlun. In the north boundary region of the plateau, the displacement vectors near north direction along the west Altyn Mountain are greater than those with northeat-southwest direction along the east Altyn Mountain. The displacements in the east-north-east direction along the Qilian mountains are also less than those in the Tibetan plateau. The displacement vectors along the southern boundary are much greater than that along the northern boundary of the plateau on an average as shown in Figure 8. It suggests that the Tibetan Plateau is undergoing a shortening along nearly N-S direction.

The displacement vectors lie nearly in the N-S direction in the west plateau and the west Kunlun. The eastward horizontal components of displacement vectors are medium in the central plateau, however, evidently greater than in the western region of the plateau. The horizontal components of displacements lie identically near the east direction on the eastern boundary of the Tibetan plateau, in the east China. The east components of displacements on the eastern boundary of the plateau are much greater than in the central Tibetan Plateau. The eastward horizontal displacement components increase on average from the west plateau to the eastern margin of the plateau, through the central plateau. The above analyses based on GPS data observed at the surface imply that there exists the southeastward crustal movement in the central plateau. This southeastward clockwise rotation is unknown but entirely possible, because east-west contraction is suggested in the western Mynmar based on numerical kinematic model (England and Molnar, 1997). From the analysis of GPS vectors, it seems that extruding Tibetan crust is neither overriding South China nor pushing it out over a free boundary in the South China Sea but extruding along southeast Asia. This result is consistent with that derived from the earthquake source mechanisms.

6. Finite element modeling

The magnitude and orientation of the tectonic stresses in the India-Eurasia collision zone are predicted by using an elastic FE program package (Hayashi, 2007) as shown in Figures 9 and 10 and Table 2. The finite element grid consists of 2424 constant strain elements interconnected by 1286 nodes. In this calculation, several sets of finite element models are constructed which treat the Himalayan-Tibet orogen as a plate like structure with both homogeneous and heterogeneous elastic rheology. A plane stress approximation is adopted for the calculation of the regional horizontal stress field. At this point, it is emphasized that the calculations ignore several possible stress sources, which might significantly influence the stress pattern in the region. It is well-known fact that topography, buoyancy forces and rheological stratification of the lithosphere can generate additional stresses, this study simply neglect those factors because this modeling mainly aims to simulate present day stress to understand contemporary stress sources and plate kinematics in the India-Eurasia collision zone. Further, it is beyond the scope of this

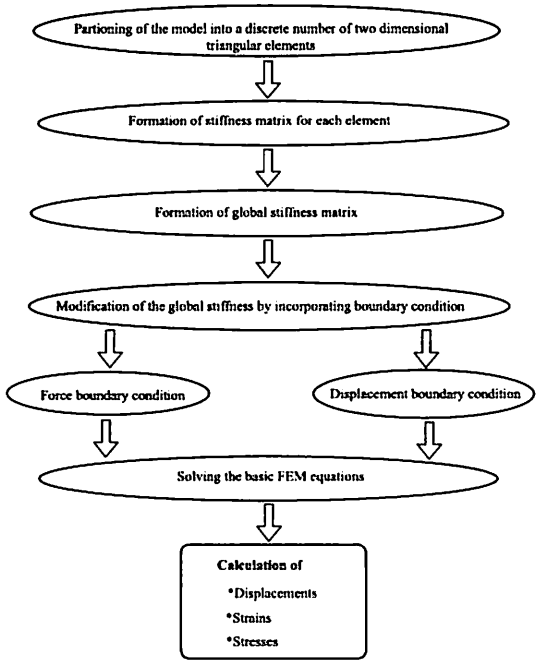

Fig.9. Flow chart of finite element modeling

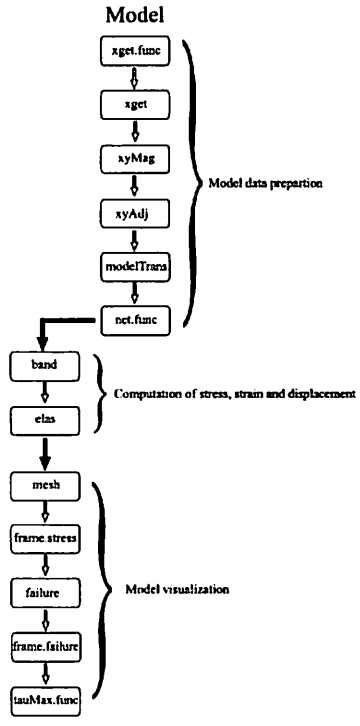

Fig.10. Software flow chart for finite element software package (Hayashi, 2007).

Table.2. Contents of finite element software package (Hayashi, 2007).

no.	code name	function
1	xget.func	raw coordinate for each nodal points in model
2	xget	coordinate data for model
3	xyMag	scale adjustment according to model size
4	xyAdj	coordinate adjustment of model's boundaries
5	modelTrans	calculation of coordinates, nodal points and layers
6	net.func	visualization of model's mesh
7	band	calculation of band matrix
8	elas	computation of stress, strain and displacement
9	mesh	division of model into layers
10	frame.stress	visualization of stress field
11	failure	computation of failure element
12	frame.failure	visualization of failure element
13	tauMax.func	calculation of shear stress

modeling to study inelastic deformation. However, this relatively simple and straightforward finite element models are quite useful in recognizing and interpreting the gross features of stress-strain relationships in the Himalaya-Tibet orogen. Such modeling

approximation has been proved to provide reliable results predicting realistic maximum horizontal compressive stress (Grunthal and Stromeyer, 1992; Bada et al., 1998; Pascal and Gabrielsen, 2001; Jarosinski et al., 2006).

6.1. Model structures and boundary conditions

Considering various tectonic features and plate kinematics, three model geometries for

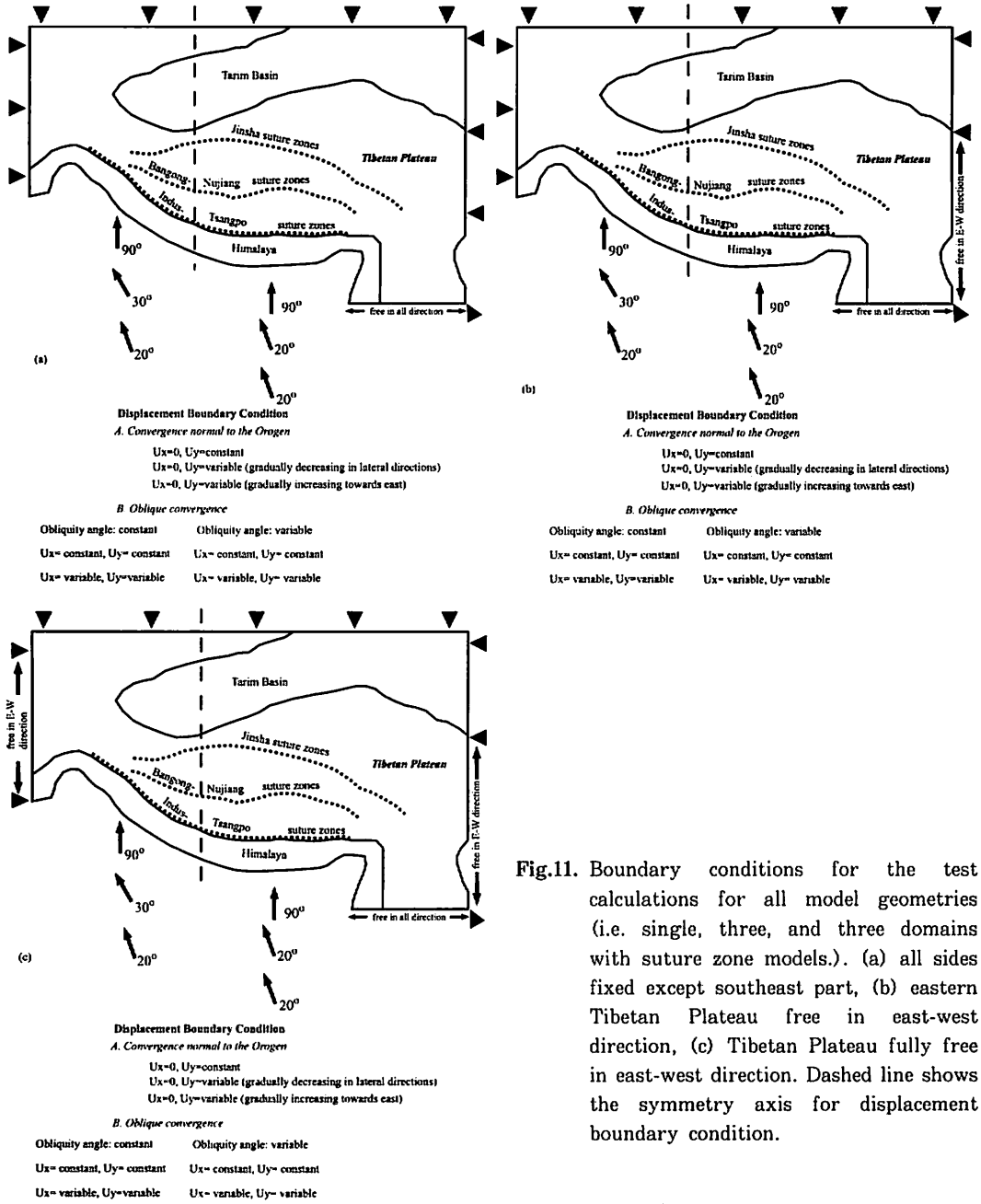

Fig.11. Boundary conditions for the test calculations for all model geometries (i.e. single, three, and three domains with suture zone models.). (a) all sides fixed except southeast part, (b) eastern Tibetan Plateau free in east-west direction, (c) Tibetan Plateau fully free in east-west direction. Dashed line shows the symmetry axis for displacement boundary condition.

the India-Eurasia collision zone are considered, they are (1) single domain homogeneous elastic plate (2) three domains heterogenous elastic plate without tectonic discontinuity and, (3) three domains elastic plate with major tectonic discontinuities. These geometries are considered to get realistic stress pattern considering effect of model geometry, variation of mechanical strength, and tectonic discontinuities in the Himalayan-Tibet orogen. The southern boundary of the model is plate boundary between Indian and Eurasian Plates i.e., Himalayan front, northern boundary is considered north of the Tian Shan mountain belt and north of Tarim basin. The western boundary is extended up to Pamir range and the eastern boundary is confined to the Ordos block to the northern side and Yangtze block to the southern side. Two sets of displacement boundary condition are imposed for all model geometries, first convergence normal to the orogenic belt, and

Table.3. Modeling features for single domain model.

Model	Displacement Boundary conditions	Depth (km)	
1	Convergence normal to orogen	10	20
2	Laterally decreases from the center	10	20
3	Gradually increases towards east	10	20
4	Oblique convergence (E:20°; W:30°) Disp: constant	10	20
5	Oblique convergence (E:20°; W:30°) Disp: variable both E-W and N-S direction	10	20
6	Oblique convergence (E:20°; W:20°) Disp: variable both E-W and N-S direction	10	20
7	Oblique convergence (E:20°; W:20°) Disp: constant for both E-W and N-S direction	10	20
8	Same as 1 but part of eastern side free in EW	10	20
9	Same as 2 but part of eastern side free in EW	10	20
10	Same as 3 but part of eastern side free in EW	10	20
11	Same as 4 but part of eastern side free in EW	10	20
12	Same as 5 but part of eastern side free in EW	10	20
13	Same as 6 but part of eastern side free in EW	10	20
14	Same as 7 but part of eastern side free in EW	10	20
15	Same as 8 but part of western side also free in EW	10	20
16	Same as 9 but part of western side also free in EW	10	20
17	Same as 10 but part of western side also free in EW	10	20
18	Same as 11 but part of western side also free in EW	10	20
19	Same as 12 but part of western side also free in EW	10	20
20	Same as 13 but part of western side also free in EW	10	20
21	Same as 14 but part of western side also free in EW	10	20
22	Same as 1 but free only along EW in SE part	10	20
23	Same as 22 but part of east and west side free along EW	10	20
24	Same as 23 but northern side free along EW	10	20

Table.4. Modeling features for three and three domains with suture zones models.

Model	Displacement Boundary conditions	Depth (km)		
1	Convergence normal to orogen	10/20/10	20/40/20	35/70/35
2	Laterally decreases from the center	10/20/10	20/40/20	35/70/35
3	Gradually increases towards east	10/20/10	20/40/20	35/70/35
4	Oblique convergence (E:20°; W:30°) Disp: constant	10/20/10	20/40/20	35/70/35
5	Oblique convergence (E: 20°; W:30°) Disp: variable both E-W an N-S direction	10/20/10	20/40/20	35/70/35
6	Oblique convergence (E:20°; W:20°) Disp: variable both E-W and N-S direction	10/20/10	20/40/20	35/70/35
7	Oblique convergence (E:20°; W:20°) Disp: constant for both E-W and N-S direction	10/20/10	20/40/20	35/70/35
8	Same as 1 but part of eastern side free in EW	10/20/10	20/40/20	35/70/35
9	Same as 2 but part of eastern side free in EW	10/20/10	20/40/20	35/70/35
10	Same as 3 but part of eastern side free in EW	10/20/10	20/40/20	35/70/35
11	Same as 4 but part of eastern side free in EW	10/20/10	20/40/20	35/70/35
12	Same as 5 but part of eastern side free in EW	10/20/10	20/40/20	35/70/35
13	Same as 6 but part of eastern side free in EW	10/20/10	20/40/20	35/70/35
14	Same as 7 but part of eastern side free in EW	10/20/10	20/40/20	35/70/35
15	Same as 8 but part of western side also free in EW	10/20/10	20/40/20	35/70/35
16	Same as 9 but part of western side also free in EW	10/20/10	20/40/20	35/70/35
17	Same as 10 but part of western side also free in EW	10/20/10	20/40/20	35/70/35
18	Same as 11 but part of western side also free in EW	10/20/10	20/40/20	35/70/35
19	Same as 12 but part of western side also free in EW	10/20/10	20/40/20	35/70/35
20	Same as 13 but part of western side also free in EW	10/20/10	20/40/20	35/70/35
21	Same as 14 but part of western side also free in EW	10/20/10	20/40/20	35/70/35
22	Same as 1 but free only along EW in SE part	10/20/10	20/40/20	35/70/35
23	Same as 22 but part of east and west side free along EW	10/20/10	20/40/20	35/70/35
24	Same as 23 but northern side free along EW	10/20/10	20/40/20	35/70/35

second, oblique convergence and are applied in the following ways (Fig. 11):

A. Convergence normal to the orogen

- Ux =0, Uy=constant
- Ux =0, Uy=variable, higher at central part and gradually decrease in lateral direction
- Ux =0, Uy=variable, gradually increasing towards east

B. Oblique convergence

a. Obliquity angle variable

- Ux =constant, Uy =constant, Angle: 20° east side, 30° west side
- Ux =variable, Uy = variable, Angle: 20° east side, 30° west side

b. Obliquity angle constant

- Ux =variable Uy = variable, Angle: 20°

● Ux =constant, Uy =constant, Angle: 20°

Although we tried all above-mentioned displacement boundary conditions (Tables 3 and 4), we obtained reasonable results only in convergence normal to the orogen. Therefore, we selected this displacement boundary condition for all model geometry. Finally, we have applied three types of boundary conditions to simulate existing plate kinematics

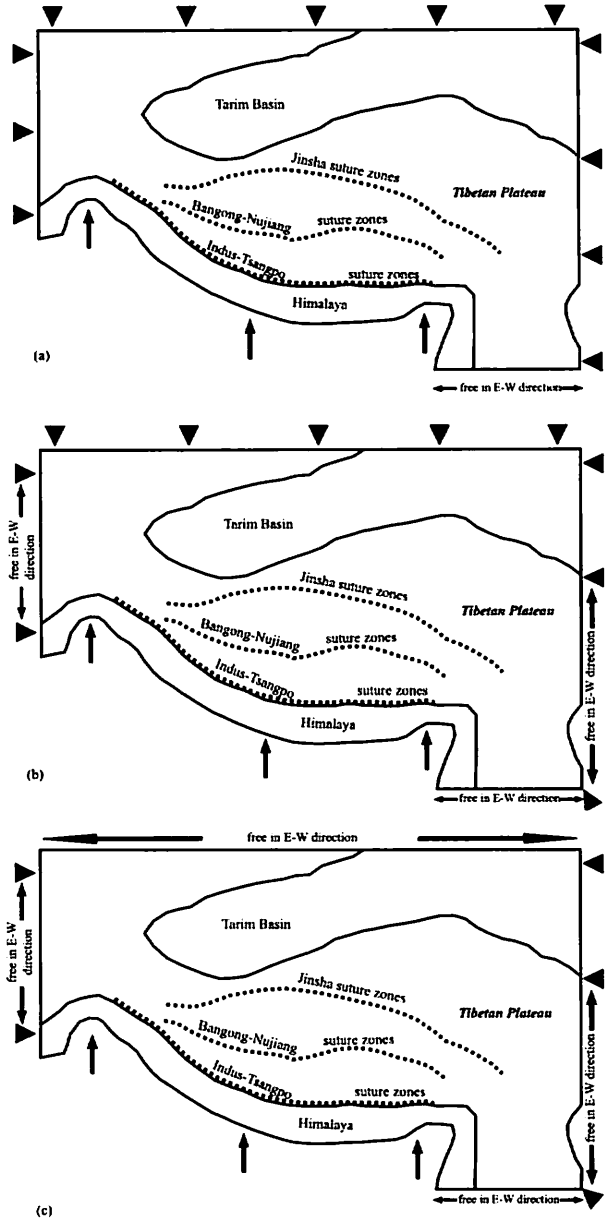

Fig.12. Boundary conditions adopted for final computation for all model geometries (a) first boundary condition (B1) (b) second boundary condition (B2) (c) third boundary condition (B3). (For all models i.e. single, three, and three domains with suture zone)

considering various possibilities. In the first boundary conditions (B1), we considered convergence displacement from the southern side of the model equivalent to shortening due to continuous convergence of the Indian Plate against Eurasian Plate. Remaining all sides is fixed in all direction except southeastern part, which is allowed to move in east-west direction (Fig. 12a). For the second boundary condition (B2), to simulate east-west extrusion of Tibet, part of the eastern and western boundaries is free in east-west direction but fixed in north-south direction (Fig. 12b). This model simulates the eastward extrusion of the Tibet. For the third boundary condition (B3), part of eastern, western, and northern boundaries are allowed to move in east-west direction but fixed to north-south direction (Fig. 12c). This geometrical boundary condition nearly reproduces E-W extrusion of the elevated Tibetan Plateau.

6.2. Rock layer properties

In this simulation, we only consider upper elastic crustal layer of the region. Therefore, elastic rheology is considered for the entire region. For the single domain model, homogeneous material property is considered as shown in Fig. 13. However, considering rigidity of the crustal blocks we allocate different values of elastic parameters for each block according to their strength contrast. The higher rigidity means higher value of elastic parameters. The elastic parameters for the three domains model are shown in Fig. 13. These parameters are not lab determined values but taken as average values for the continental crustal rocks as used by several modelers in various region on the globe (Grunthal and Stromeyer, 1992; Bada et al., 1998; Jarosinski et al., 2006). Several test models are run to understand relative effect of variation of rock layer properties on the computed stress field. It is observed that there is little or no sensitivity of the absolute magnitude of the elastic parameters. For the tectonic discontinuities, we are biased to use

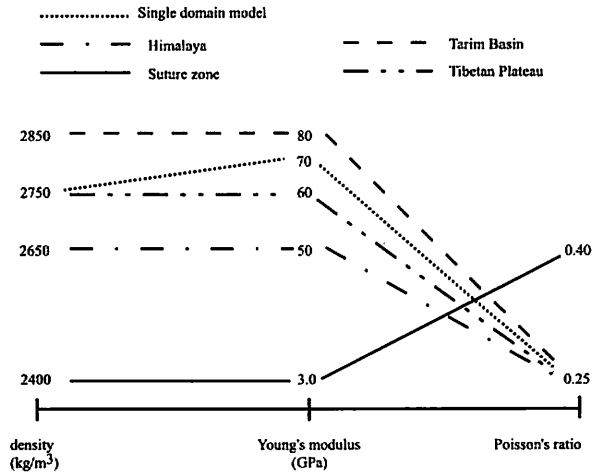

Fig.13. Rock layer properties adopted for the calculation.

Young's modulus ~3 GPa as used by Homberg et al. (1997). We used higher value for the Tarim basin and other low land areas because these areas behave like a strong rigid body as shown by strain data, GPS data and other modeling findings.

7. Modeling Results

7.1. Stress field

Considering model geometry, various boundary conditions, and effect of changing crustal depth, series of models are run to simulate the reliable stress field in the Himalaya-Tibet orogen. In the next section, we discuss all models according to factors that affect the contemporary stress field in the region.

7.1.1. Relative influence of imposed boundary condition

It is obvious that model geometry and boundary condition are important factors that affect the stress field in all kind of geodynamic modeling. As mentioned before, in this work, we consider two kinds of model geometry; first, homogeneous model consisting of single elastic domain, and second, three domains model constituting Himalaya, Tibetan Plateau and adjacent areas.

For all models, several displacement boundary conditions were tested as mentioned-above. Only convergence normal to the orogen was found to be more relevant to simulate present day stress field in the Himalaya-Tibet region. In case of geometrical boundary condition, as mentioned before, three sets of condition are applied; first B1 condition, western, eastern, northern sides of the model are fixed in all direction and southeastern boundary is permitted to move in east-west direction. Uniform convergent displacement (2000m) is applied from the southwestern part of the model in accordance with the kinematics of the Indian plate (Fig. 12a). Secondly, B2 condition; to allow the EW tectonic escape from the plateau, parts of the eastern and western boundaries are allowed to move in E-W-direction. Other conditions are same as above (Fig. 12b). Thirdly, B3 condition northern boundary is permitted to move in east-west direction and remaining all sides share the similar situation as in the second boundary condition (Fig. 12c).

For the single domain model, at first 10 km crustal depth is considered along with first boundary condition (B1; Fig. 12a). The simulated maximum compressive horizontal stress (σ_{Hmax}) has shown three orientations in different regions of the Himalaya-Tibet orogen. In the eastern syntaxis, stress field is oriented towards northeast. This region has clearly shown the clockwise rotation of the simulated σ_{Hmax} (Fig. 14a). To the southeastern part, stress field is of tensional type and are oriented almost along the north-south direction. However, to the western syntaxis, direction of σ_{Hmax} is drastically changed. It clearly shows the counter clockwise rotation. The direction of σ_{Hmax} in eastern sector of the Himalaya is perpendicular to the orogen, i.e. northwest direction and is gradually change

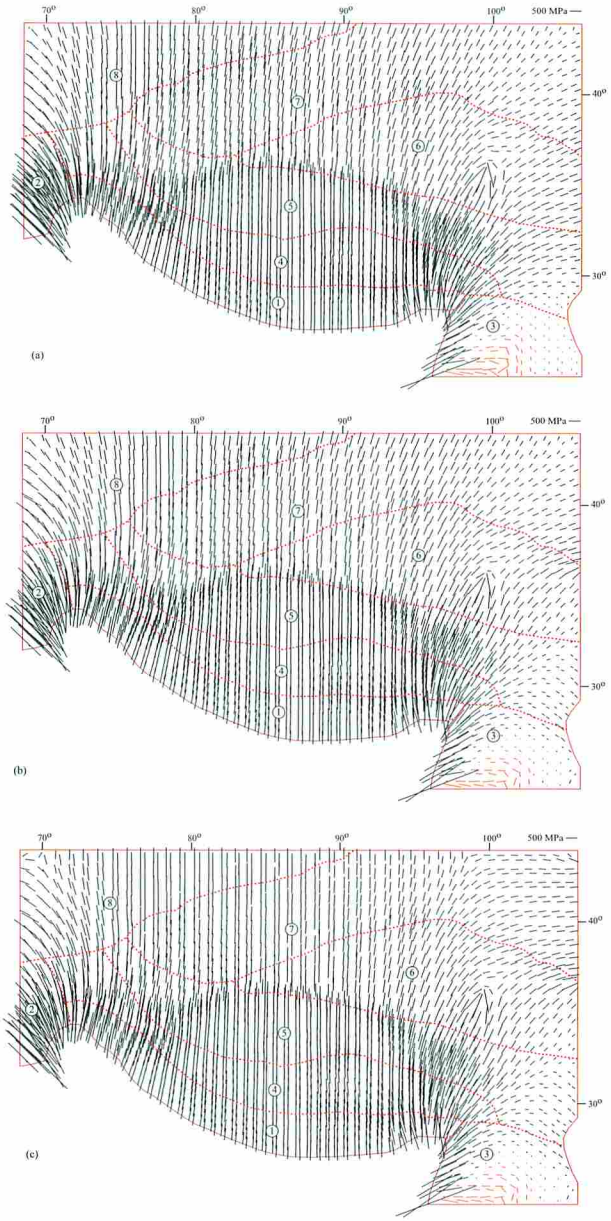

Fig.14. Calculated contemporary maximum horizontal compressive stress (σ_{Hmax}) for a single domain elastic crustal plate for boundary conditions (a) B1 (b) B2 (c) B3. Red bar shows tensional stress. Hereafter in all models areas shown by dotted red lines are tentative stress provinces and do not correspond to domains. 1. Himalaya, 2. Western syntaxis, 3. Eastern syntaxis, 4. Southern Tibet, 5. Central Tibet, 6. Northern Tibet, 7. Tarim basin and lowland areas, 8. Tian Shan.

towards north in southern Tibet, which further deviates towards north-east in the central and northern Tibet. To the northeastern part of the Tibetan Plateau and around the

Tarim basin and lowland areas σ_{Hmax} changes its direction from north to northeast. In contrast to eastern sector of the Himalaya, the orientation of the σ_{Hmax} in western sector of the Himalya is directed towards northeast and gradually turns to the northwest in southern Tibet, central Tibet and Pamir region. In the central Tibetan Plateau, σ_{Hmax} is almost in north-south orientation. Overall features show the fan shape distribution of the σ_{Hmax}. The magnitude of the maximum compressive stress varies from place to place. Relatively higher magnitude is observed in the Himalayan orogen, eastern and western syntaxes. There is gradual decrease in magnitude to the northern part of the Tibetan Plateau and southeastern part of the model (Fig. 14a). In case of second boundary condition (B2; Fig. 12b), significant changes occur in orientation of the computed σ_{Hmax}. The computed σ_{Hmax} in the southeast and around northeast of Tarim basin is strongly rotated in clockwise manner as compared to previous model (Fig. 14b). Similar effect of this boundary condition is also observed to the western part of the model, where degree of rotation is relatively higher. As we imposed the third boundary condition (B3, Fig. 12c), σ_{Hmax} shows different pattern. The orientation of σ_{Hmax} trajectories varies drastically in the eastern boundary of the Tibetan Plateau. To the north of Tibetan Plateau, σ_{Hmax} are aligned along E-W direction. However, in the eastern part of northern and central Tibetan Plateau, σ_{Hmax} are oriented towards northeastern direction with lower deviation to that of B1 boundary conditions (Figs. 14a and c). However, this orientation is gradually changed due to strong clockwise rotation of σ_{Hmax} in the southeast (Fig. 14c). Nevertheless, there is almost no change in orientation of σ_{Hmax} in the central part of the model, i.e. Himalaya and Tibetan Plateau. Overall results indicate that the single domains model cannot simulate the contemporary stress field of the region. From afore-described models, it is realized that stress field in the Himalayan-Tibet orogen is controlled by tectonic boundary conditions and geometry of the tectonic domains.

In the second set of model, to realize the effect of material inhomogenity, we divided entire modeled area into three regions representing Himalaya, Tibetan Plateau, and Tarim basin, and other low land areas. The crustal depths are assigned as 10 km for the Himalaya, 20 km for the Tibetan Plateau and 10 km for the Tarim basin. In this case also, we imposed all three boundary conditions. In first boundary condition (B1, Fig. 12a), orientation of σ_{Hmax} and its state is different because of material inhomogeneity. To the eastern part of the central and northern Tibetan Plateau, computed σ_{Hmax} is oriented in east-west direction and is changed to almost northwest-southeast direction to the southern part (Fig. 15a). This feature is consistent with the observed σ_{Hmax} (Figs. 6 and 15a). Towards northern part of the Tibetan Plateau, σ_{Hmax} is oriented towards northeast direction at lower angle as compared to southern part. To the western syntaxis, Pamir and Tian Shan area, σ_{Hmax} are oriented towards northwestern, which is consistent with the observed σ_{Hmax} data. In the central sector of the model, it gives north-south orientation of σ_{Hmax}. The σ_{Hmax} trajectory in the eastern Himalaya, first oriented perpendicular to the

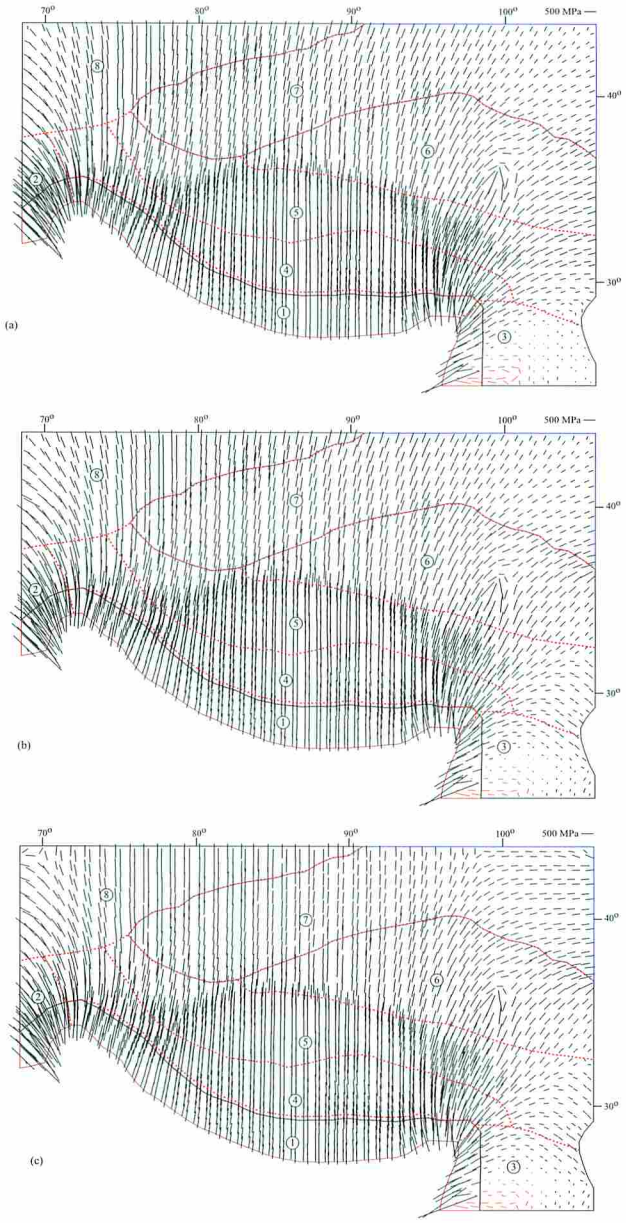

Fig.15. Calculated contemporary maximum horizontal compressive stress (σ_{Hmax}) orientations for the three domains elastic crustal plate for boundary condition (a) B1 (b) B2 (c) B3. Red bar shows tensional stress.

orogen and gradually turns to the northeast from central Tibet to onwards. Similarly, to the western sector of the Himalaya, σ_{Hmax} makes its trajectory normal to the orogen and it rotates towards northeast and finally deviates towards northwest. Significantly, in this model σ_{Hmax} is deviated from its position as it passes from less competent to competent rocks as it seen in Tarim basin and Tibetan Plateau (Fig. 15a). In the second boundary

condition (B2, Fig. 12b), orientation of σ_{Hmax} is almost similar to that of single layered model. The direction of σ_{Hmax} is different to that of first boundary condition, i.e., it strongly rotates in clockwise manner and finally aligned towards southeast directions (Fig. 15b) in the eastern part of the central Tibet and eastern syntaxis, remaining all stress characteristics almost similar to that of the single domain model. In the third boundary condition (B3, Fig. 12c), to the eastern part of the Tarim basin, computed σ_{Hmax} are oriented in east-west direction (Fig. 15c), which is not consistent with the observed σ_{Hmax}.

7.1.2. Effect of suture zones in the Himalaya-Tibet orogen

Three suture zones are incorporated into the finite element model to simulate possible effect of these presently active tectonic discontinuties. Although there are many active faults, for simplicity we consider only the major suture zones from south to north, they are Indus-Tsangpo, Bangong-Nujiang and Jinsha suture zones. These tectonic discontinuties also represent major boundary between the crustal blocks in the Tibetan Plateau. In the model, these suture zones are considered as weak zone so that relative movement is possible and crustal deformation due to ongoing collision can be accounted. Various crustal depths are considered, i.e., 10 km for the Himalaya and Tarim basin and 20 km for the Tibetan Plateau and suture zones. The first boundary condition (B1, Fig. 12a) shows realistic stress field in which σ_{Hmax} has been changed due to the presence of crustal-scale tectonic discontinuities (Fig. 16a). The effect of discontinuities is more pronounced in the Tarim basin and other associated lowland areas, where field observation shows thinner crust than the Tibetan Plateau. These areas are characterized by relatively lower magnitude of σ_{Hmax} (Fig. 16a). To the eastern syntaxis, σ_{Hmax} are aligned to the east and is gradually change to northeast in the eastern part of the Tibetan Plateau. To the eastern syntaxis, direction of σ_{Hmax} is toward south-southeast, which shows the satisfactory orientation with the observed σ_{Hmax} (Figs. 16a and 6). However, in the western syntaxis and adjoining areas, σ_{Hmax} is aligned towards northwest. In the central sectors of the Himalaya, trend of σ_{Hmax} is north-south and is laterally deviates towards northwest and northeast giving fan-shaped distribution of σ_{Hmax} (Fig. 16a). By changing boundary conditions, there are no significant changes in orientation of the σ_{Hmax} as compared to predicted σ_{Hmax} for three domains models (Figs. 15a-16c,). In summary, incorporation of suture zone does not significantly change σ_{Hmax} orientation except slight decrease in stress magnitude.

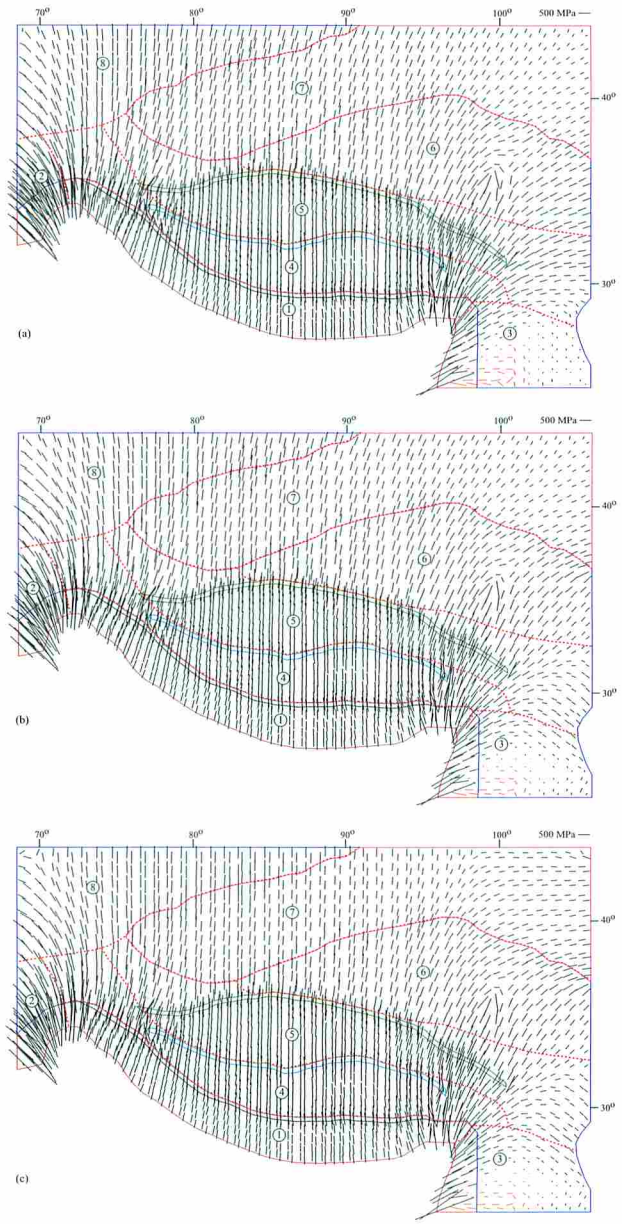

Fig.16. Calculated contemporary maximum horizontal compressive stress (σ_{Hmax}) orientations for the three domains elastic crustal plate with major suture zones for boundary condition (a) B1 (b) B2 (c) B3. Red bar shows tensional stress

7.1.3. Effect of changing crustal depth

As we know that crustal thickness greatly affects the stress magnitude and direction, therefore, to understand variation of stress magntitude and direction, several models are run using different model geometry and crustal depth. To this state, it is clear that out

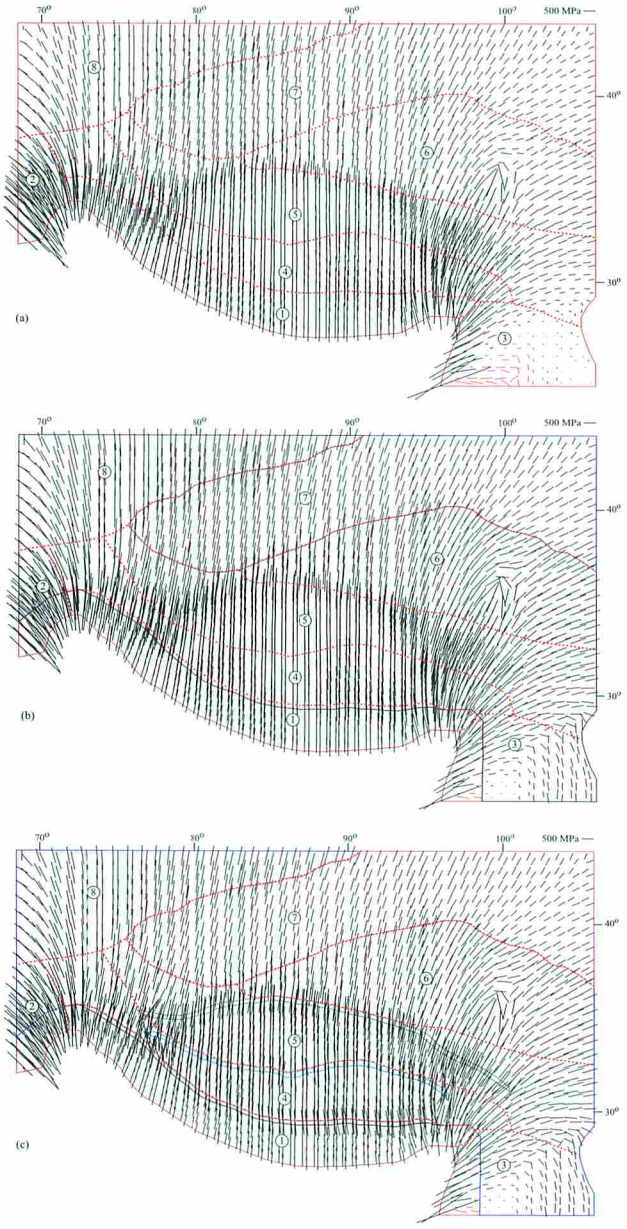

Fig.17. Calculated contemporary maximum horizontal compressive stress (σ_{Hmax}) orientations showing the effect of crustal depth in the study area for boundary condition (B1) (a) single domain (b) Three domains (c) Three domains with major suture zones. Red bar shows tensional stress.

of three applied boundary conditions, first boundary condition (B1, Fig. 12a) can satisfactorily reproduce observed σ_{Hmax} for the Himalayan-Tibet region. Therefore, in this section we show only models with first boundary condition with increasing crustal depth. For the single domain model, we considered 20 km depth for the entire region. The

computed σ_{Hmax} has more pronounced orientation and magnitude of σ_{Hmax} has been little bit increased as compared to the shallow depth model. Similarly, more compressive stress regime is observed in the southeastern region (Fig. 17a). For the three domains model, we consider variable depth, i.e. 35 km for the Himalaya, 70 km for the Tibetan Plateau and 35 km for the Tarim basin and other low land areas. These depths distribution are more or less consistent with the observed crustal thickness in the Himalayan-Tibet region. In comparison to shallow crustal depth (Figs. 14a, 15a, 16a and 17), this model gives more realistic stress pattern because of the stress amplification due to crustal depth. The orientation of σ_{Hmax} in the southeast is almost in southeast direction in compressive regime (Fig. 17b). This pattern reconciles with the observed orientation of the σ_{Hmax}. Other patterns remain same as in shallow crustal depth model. With the inclusions of major tectonic discontinuities, stress field around the tectonic discontinuities is slightly perturbed. This perturbation is due to competency contrast between the adjoining blocks (Fig. 17c). Overall results do not show significant changes on orientation. However, magnitude and state of the σ_{Hmax} are found to be controlled by depth variation.

7.2. Displacement field

Although comparison of computed displacement field with GPS data is not prime objective of this research, therefore, we simply compute to understand general trend. Since the first boundary condition gives us realistic stress field, displacement vector map for this condition is described here. The computed displacement field is almost similar for different model geometry (Fig. 18). For the single domain model, (Fig.18a) displacement vectors in the eastern half of the model are normal to the orogen and gradually deviate towards northeast direction from the central Tibet finally trending to east. To the western sector of the model, however, displacement vectors are oriented in north south direction. Magnitude of displacement vector decreases towards north. Similar pattern can be observed in three domains model (Fig.18b). Inclusion of suture zone does not significantly change orientation of displacement vector (Fig.18c). Qualitatively, obtained displacement vector partially consistent except southeastern part, where displacement vectors are in opposite direction to that of GPS data. One possible reason for inconsistency is we consider only the effect of the India-Eurasia collision. However, we did not consider gravitational potential energy difference of the Tibetan Plateau and shear traction on the bottom of the lithosphere induced by the global mantle convection and plate kinematics in southeast Asia which may have influence on crustal deformation.

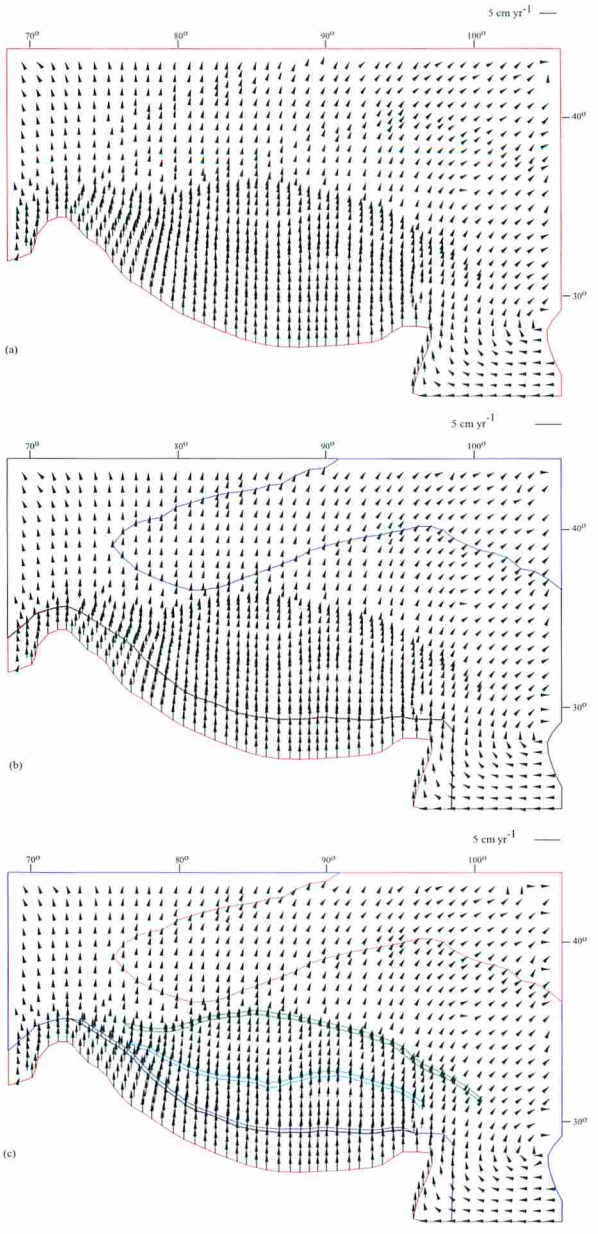

Fig.18. Displacement vector for B1 boundary condition. (a) single domain (b) three domains, and (c) three domains with suture zones model.

8. Discussion

8.1. Model set up and rheology

A number of models have been presented, which demonstrate the relative importance of the various geometry, displacement boundary conditions and tectonic discontinuties on

stress field of the India-Eurasia collison zone. Various relative boundary conditions are used with continuous convergence of the Indian Plate to Eurasian Plate. To get better understanding on the lateral inhomogenity of the crustal blocks and its relative influence on the stress field, three kinds of models are produced, i.e. single domain model, three domains models with inhomogenity on mechanical parameters and block models with inclusion of major suture zones. Linear elastic rheology is considered for the continental crust of the Himalaya-Tibet orogen. The consideration of elastic rheology is an oversimplification, however, it is justifiable in the present study with the emphasis on modeling the regional stress field, which is due to time-independent sources (e.g. convergent displacement, lateral inhomogenity of the material properties, and topography related forces) and can be considered to be in steady state. The modeling approach adopted in this study, therefore, is justifiable to simulate the first order stress field in the collison zone between the Indian and Eurasian plates.

8.2. Comparison of models with the observed stress data

The computed models show that general trend of the recent stress field in the Himalayan-Tibet orogen can be simulated by applying relatively simple but geologically reasonable boundary conditions. The models comprise the deformation of crustal blocks with different geometry and rigidities in the convergent setting, i.e. active collision zone between Indian and Eurasian plates. A direct comparison between computed σ_{Hmax} and observed σ_{Hmax} data is difficult because of scattered data set especially for the Tarim basin and other lowland areas. To allow a more meaningful comparison, observed data were compared with the smoothed σ_{Hmax} stress map produced using interpolating and extrapolating technique of Muller et al. (2003).

Several boundary conditions with three types of model geometry have been tested to reproduce present day σ_{Hmax} orientation. The computed stress field in the Himalaya-Tibet region is controlled by the tectonic boundary condition and model geometry rather than the material properties. The single domain model with lower crustal depth can give poorly matched σ_{Hmax} orientation and stress regime. In the first boundary condition, σ_{Hmax} give fan-shaped orientation. This model fails to simulate southeast oriented maximum horizontal compressive stress north of the Indo-Burmese collision zone. The simulated σ_{Hmax} is entirely tensional in nature, which contradicts observed data. For the second boundary condition, computed σ_{Hmax} rotated strongly in clockwise direction even aligned in east-west direction and are not matched with the observed data. In third boundary condition, where northern part of the model and part of the eastern and western boundary of the model are free to move in east-west direction can mimic the kinematics required for the eastward extrusion of the Tibetan crust. However, the computed stress field for this kinematics is not reasonable. Therefore, it is clear that present day stress field is not due to eastward tectonic escape of the Tibetan plateau. The three domains

model with B1 boundary condition reproduces consistent results that can be comparable with the measured σ_{Hmax} direction. This boundary condition is consistent with the kinematics derived from the GPS data (Wang et al., 2001). The models with heterogeneous material properties show consistent results because of perturbations of σ_{Hmax} orientation in areas of juxtaposed strong and weak rheologies. To the western sector of the model, in and around the Pamir and Hindu-Kush region, computed σ_{Hmax} shows northwest trend, which reconciles the observed data. The stress state determined from the focal mechanism data shows mixed types of strike-slip and thrust types earthquakes. Unfortunately, there are no GPS data, however, geological and geophysical observations indicate that the Pamir Plateau and Hindu-Kush range act as rigid block obstructing the convergence between Indian and Eurasian plates. The simulated stress pattern in and around Tarim basin, which is considered as a rigid block having high mechanical strength, shows deviation in computed σ_{Hmax}. The computed σ_{Hmax} is oriented towards northeast direction. However, the magnitude of σ_{Hmax} is lower for this region because mechanical strength is higher and is less deformed in response to force due to convergence of Indian Plate. Therefore, this block might have been playing a role of strong backstop to obstruct northward convergence of the Indian plate so that the entire Tibetan Plateau is moving towards southeast. This kinematics further enhanced by the Altyn Tagh fault. The magnitude of σ_{Hmax} is smaller for this area. In addition, there are few seismic events of thrust types, therefore, this area is considered as the strong backstops with active compressional deformation. North of the Tarim basin, Tian Shan belt has been experiencing frequent thrust type earthquakes indicating its active deformation. The computed σ_{Hmax} direction for this region is compressive and is consistent with the observed data. To the northeast, around North China and Ordos block, σ_{Hmax} trend is towards northeast and are of compressive nature. This area is characterized by the compressive deformation as shown by thrust type earthquakes. Simulated orientation of σ_{Hmax} gives good correlation with the observed data. Further GPS vector shows deviation towards southeast and low horizontal velocity 2-8 $mmyr^{-1}$ (Wang et al., 2001). This gradual decrease in GPS velocity and its deviation are probably due to rigid nature of the Ordos block, which consequently produces northeast oriented σ_{Hmax}. On the basis of stress field deviation and GPS data, it can be said that northern region of the model area, e.g. Tian Shan, Tarim Basin and North China including Ordos block behave as a rigid backstop to obstruct influence of the convergence of the Indian Plate. The eastern part of the Tibetan Plateau shows two orientations of σ_{Hmax} in the first boundary condition. First northeast oriented compressive σ_{Hmax} up to Ordos block, and second, almost east-west trending stress field. The focal mechanism data show almost strike-slip events with east-west orientation of σ_{Hmax} and few thrust type events in Longmen Shan area. These observations are consistent with the computed σ_{Hmax} for the region. However, to understand relative influence of the eastward tectonic escape on present day stress field, we have imposed two more boundary conditions

(B2 and B3) as explained in the previous section, the predicted σ_{Hmax} and their orientation do not match with the present day data. Further, recent GPS data indicate that velocity decreases towards South China and average value is of 6 to 11 mmyr^{-1} toward an azimuth N100o-130oE (Wang et al., 2001). These data predict that the South China block behaves as a rigid block without internal deformation. In this regard, on the basis of computed σ_{Hmax} orientation, it is clear that South China acts as a rigid block rather than transmitter of the extrusion of the elevated Tibetan Plateau. For the southeastern part, i.e. around Indo-Burmese arc, computed σ_{Hmax} are oriented towards southeast and are compressive in nature with few tensional stresses. Frequent occurrence of strike-slip earthquakes reflectes the active crustal deformation in and around the Indo-Burmese arc. In the model, I allowed to move southeastern part in E-W direction and fixed to N-S direction. This kinematics fairly simulated the stress field of the region. The present day kinematics of this region is consistent with the adopted boundary condition. The GPS vectors for this region are aligned towards southeast and magnitude is comparatively higher to that of the North China and South China. Interestingly, in the Himalayan front and adjoining syntaxes, σ_{Hmax} shows fan-shaped distribution. It shows clockwise rotation to the eastern syntaxis and counter clockwise rotation to the western syntaxis. This is probably due to indentation of strong Indian lithosphere to the relatively soft Eurasian lithosphere. The computed σ_{Hmax} more or less match the observed stress field in the area. Therefore, indenter model is probably best to describe observed deformation in the Himalaya-Tibet orogen. The overall kinematics is able to say that present day stress is outcome of the continuous convergence of the Indian plate to the semi-close system of the Tibetan Plateau and adjacent areas.

Recently, there are two schools of thought for the active deformation of the Himalaya-Tibet region, one believe that active deformation of the region is due to lateral extrusion of rigid blocks via large strike-slip faults which accommodates most of the convergence between India-Eurasia and the other believe that the deformation is not like that manner but due to crustal shortening and thickening by which crustal flow continues in the region. Later believe that continuum tectonics (England and Houseman, 1986; Shen et al., 2001) is active rather than the block tectonics (Molnar and Tapponier, 1975; Replumaz and Tapponier, 2003; Chen et al., 2004; Thatcher, 2007) for the current deformation of the region. Each end member model can explain some observed data but neither is completely satisfactory. In this regard, we tried both end members considering sutures as weak zones to separate entire model area into different blocks. The simulated models are not differentiable because simulated σ_{Hmax} do not differ greatly except slight perturbation in orientation and slight decrease in magnitude for the model with suture zones. Therefore, considering my modeling results, we prefer continuum tectonics rather than block tectonics.

Significant change of crustal thickness in and around the India-Eurasia collision zone is

observed. Such variation in crustal thickness greatly affects the crustal deformation and tectonic style as observed in the different region of the Himalaya-Tibet region. Thickness and depth variations in an elastic plate can significantly influence both magnitude and the orientation of tectonic stress. Further, tectonic stress is greatly affected by the crustal depth variation such as in Himalya and Tibetan Plateau as evidenced by two contrasting tectonics govern by change in stress state. The Himalayan belt to the south is in compressional stress system whereas the elevated Tibetan Plateau to the north is largely affected by extensional tectonics. Therefore, in the present modeling we used different crustal depths to understand how stress varies according to crustal depth variation. In all models, we found that present day stress state can be simulated by incorporating crustal depths because of which stress state and orientation are changed giving best-fit model for the observed σ_{Hmax}. Figure 19 shows stress trajectories of both calculated σ_{Hmax} and sHmin giving chacteristics fan shape for former one and arcuate for the later.

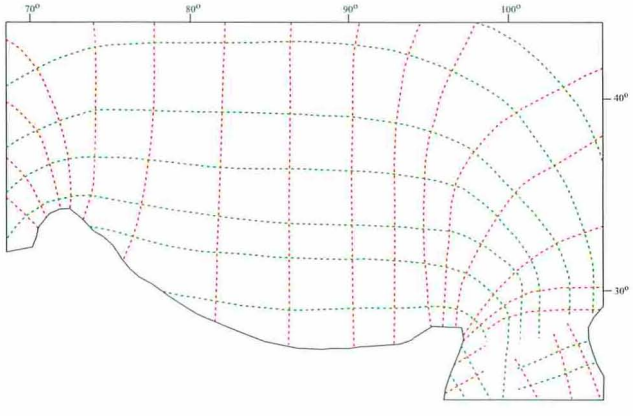

Fig.19. Calculated σ_{Hmax} (red) and sHmin (green) trajectories for the India-Eurasia collision zone.

8.3. Present day kinematics and stress sources in the India-Eurasia collision zone

Three types of tectonic deformation characterize the Himalaya-Tibet orogen, which is composed of several tectonic blocks. First, to the south of the Tibetan Plateau, entire Himalayan fold-and-thrust belt is characterized by compression tectonic environment with foreland propagation of thrust faults. This zone is considered as most active zone with propagation of deformation towards the foreland. The active deformation is reflected by several shallow to medium-depth thrust type earthquake. Second, the crest of the Himalaya is transected enigmatically by orogen parallel normal faults, STDF. Thirdly, the elevated Tibetan Plateau is deformed by several north-south trending normal faults and associated grabens and strike-slip faults. Strike-slip faults are considered to be responsible for the tectonic extrusion of the plateau. However, recently, there are different concepts on the extrusion of the Tibetan plateau. From the present modeling, it is understood that the oblique convergence is not suitable to simulate contemporary stress field. Differently,

convergence normal to the orogen can satisfactorily predict the present day stress field. However, there are several studies that used both oblique (Soofi and King, 2002) and normal (Kapp and Guynn, 2004) convergences to study geodynamic processes that are responsible for the observed deformation in Tibet. Most of the researchers define boundary conditions according to their research objectives. There is, therefore, no consistent definition of boundary condition in India-Eurasia collision zone. Considering σ_{Hmax} as a proxy, convergence normal to the orogen is essential to reproduce present day stress field. For the eastern, western, and northern side of the Tibetan plateau, the kinematics that allowed extrusion of the plateau has not given the reasonable σ_{Hmax} direction and state. Only convergence normal to the orogen along with partially free boundary condition in Southeast Asia can simulate neotectonic stress field.

The model calculations show that general trend of recent neotectonic stress is result of the convergence of the Indian Plate against the Euarsian Plate. Recent stress indicators in the Himalayan-Tibet orogen show fan-shape distribution of σ_{Hmax}. The best-fit stress field with the observed σ_{Hmax} can be obtained only if eastern, western and northern part of the model with three domains is fixed in all direction; i.e. B1 boundary condition. To the western part, the Pamir Plateau acts as a rigid block to accommodate convergence. In the northwestern part, the Tian Shan belt acts as a rigid body and acts as a secondary stress source. Further, frequent thrust type earthquakes deform this belt repeatedly. The GPS velocity field is also decreasing towards the Tian Shan indicating rigid nature of the entire mountain belt. The northern boundary consists of lowland area including Tarim basin, Qaidam basin are seismically not so active region. However, few thrust type earthquakes are observed showing compressive nature of deformation. The Tarim basin therefore acts as a rigid backstop. Similar idea has been forwarded by England and Houseman (1985) using geodynamic modeling. Northeastern part of the model, the Ordos block and surrounding area reveals gradual decrease in GPS velocity along with southeastward deviation of vectors (Wang et al. 2001). This suggests that North China and Ordos block are acting as a rigid backstop to generate compressive stress field. In the eastern part of the Tibetan plateau, present-day deformation and stress field is controlled by compressional deformation in Longmen Shan as indicated by shallow to medium thrust type earthquakes. Because of Longmen Shan, the extruding Tibetan crust neither overriding the Pacific Plate nor pushing it out over free boundary condition. Modeling results, therefore, confirm that eastern part of the Tibetan Plateau with Longmen Shan act as a rigid block enhancing generation of compressive stress field. Global positioning data are also consistent with these findings. Further southeast free boundary along the east-west simulates reliable stress field rather than fixed condition. This implies that present day extrusion of the plateau is towards southeast direction rather than the east as explained by GPS data. Therefore, imposed boundary conditions have revealed that the entire India-Eurasia collision zone is in semi-closed system as shown in Figure 20.

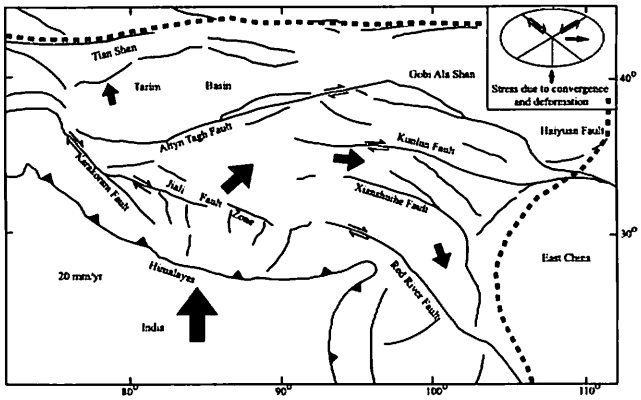

Fig.20. Sketch of present day plate kinematics in the India-Eurasia collision zone. Dotted thick-line indicates rigid boundary.

9. Conclusions

The high level of seismicity in the India-Eurasia collision zone makes it earthquakes a reliable indicator of the regional stress field. The data set documented by World Stress Map (WSM) project is good resource to study stress field in this area reflected by diverse geodynamical processes. The complex stress field in India-Eurasia collision zone can be explained by structural model with precise boundary condition and plate kinematics. This study has found that regional stress field in Himalaya-Tibet region, as shown in WSM, can be modeled using combination of convergence of Indian Plate against Eurasia and present-day tectonic boundary conditions. On these grounds, India-Eurasia collision zone provides an especially pertinent case to compare the outcomes of lithospheric regional stress modeling with stress indicator from earthquake focal mechanism data and other in-situ stress measurements. Despite several limitations and simple approach of stress modeling, results point out following key points:

1. The high level of the intercontinental stress field, the dominance of compression and the strong variation in observed maximum horizontal compressive stress (σ_{Hmax}) in different areas of the Himalaya-Tibet region are consequences of its unique geodynamic situation and tectonic boundary conditions.
2. The convergence of Indian Plate dominantly controls the magnitude and pattern of the first order stress in the Himalaya-Tibet region.
3. The direction of plate convergence is known to be an important factor because convergence normal to the orogen has given more relevant orientation of the σ_{Hmax} as compare to oblique convergence.
4. The kinematics equivalent to east-west tectonic escape did not simulate the observed stress field. Therefore, it is understood that the present day stress field is mainly governed by the southeastward tectonic escape of the Tibetan crust rather than

eastward extrusion, which is also supported by GPS data. Model with three domains and B1 boundary condition can give best-fit stress field in the India-Eurasia collision zone.

5. Geological structures have minor influence on orientation and magnitude of the σ_{Hmax}. Incorporation of suture zones in the model did not change orientation of σ_{Hmax} significantly. However, there is only small variation of magnitude of σ_{Hmax}. Further, B2 and B3 boundary conditions in which plateau is allowed to move in east-west direction did not simulate the maximum horizontal compressive stress (σ_{Hmax}). If the "block tectonic model" is suitable, there must be consistency between simulated and observed stress field in the models with suture zones and B2 and B3 boundary conditions. Considering this fact, 'continuum tectonic model' is preferred for the active deformation of the Tibetan Plateau because significant changes could not observe for the block models by incorporating suture zones as proposed by followers of "block tectonic model".
6. While the models from this study provide a reasonable interpretation of the stress orientation and seismicity observed in the India-Eurasia collision zone, some part of the model does not give good fit with the observed data. This could be due to perturbation in the stress field associated with either local or regional structures and their present movement or far field plate kinematics of the Southeast Asia.

Overall, the models presented and discussed here show that the general features of the present-day stress field in the India-Eurasia collision zone can fairly be simulated by applying relatively simple but geologically rational boundary conditions. We emphasize that simulated models ignores stress sources, which might play an important role in controlling the recent state of stress in and around the Himalayan-Tibet region. The tectonic factors, such as the effects of topography and buoyancy forces, thermal stress, and rheological stratification of the lithosphere may generate additional stresses. Nevertheless, reasonably simple models considered in this study are straightforward and important to understand neotectonic deformation in the India-Eurasia collision zone.

Acknowledgements

DC is grateful to Ministry of Education, Culture, Sports, Science, and Technology, (Monbukagakusho) Japan for the scholarship to carry out this research work under the special graduate program of the Graduate School of Engineering and Science, University of the Ryukyus, Okinawa, Japan.

References

Avouac, J.P., 2003. Mountain building, erosion, and the seismic cycle in the Nepal

Himalaya. Advances in Geophysics 46, 1-80.

Bada, G., Cloetingh, S., Gerner, P. and Horv´ath, F., 1998. Sources of recent tectonic stress in the Pannonian region: inferences from finite element modeling, Geophysical Journal International 134, 87-101.

Bilham, R.A., Larson, K., Freymuller, and project Idylhim Members, 1997. GPS measurements of of present day convergence rates in Nepal the Himalaya. Nature 336, 61-64.

Blisniuk, P. M., Hacker, B. R., Glodny, J., Ratschbacher, L., Bi, S., Wu, Z., McWilliams, M. O., and Calvert, A., 2001. Normal faulting in central Tibet since at least 13.5 Myr ago, Nature, 412, 628 - 632.

Burchfiel, B.C., Zhiliang, C., Hodges, K.V., Yuping L., Royden, L., Changrong, D. and Jiene, X., 1992. The South Tibetan Detachment System, Himalayan orogen: extension contemporaneous with and parallel to shortening in a collisional belt. Geological Society of America Special Paper, 269, 1-41.

Chamlagain, D., and Hayashi, D., 2006. Numerical modeling of graben faults with special reference to Thakkhola half-graben, central Nepal Himalaya. Himalyan Geology 27 (2), 95-110.

Chen, Q., Freymueller, Wang, Q., Yang, Z., Xu, C., and Liu, J., 2004. A deforming block model for the present-day tectonics of Tibet. Journal of Geophysical Research 109, doi:10.1029/2002JB002151.

Chen, W.-P., and Kao, H., 1996. Seismotectonics of Asia: Some recent progress, in The Tectonic Evolution of Asia, edited by A. Yin and T. M. Harrison, pp. 37 - 62, Cambridge University Press, New York.

Chen, W.P., Nabelek, J.L., Fitch, T.J., and Molnar, P., 1981. An intermediate depth earthquake beneath Tibet: source characteristics of the event of September 14, 1976. Journal of Geophysical Research 86 (B4), 2863- 2876.

Cloetingh, S. and Wortel, R., 1986. Stress in the Indo-Australian plate. Tectonophysics 132, 49-67.

Coleman, M. E., and Hodges, K. V., 1995. Evidence for Tibetan Plateau uplift before 14 Myr ago from a new minimum estimate for east west extension, Nature 474, 49-52.

DeCelles, P.G., Robinson, D.M., and Zandt, G., 2002. Implication of shortening in the Himalayan fold-thrust belt for uplift of the Tibetan Plateau. Tectonics 21, doi:10.1029/2001TC001322.

DeCelles, P.G., Robinson, D.M., Quade, J., Ojha, T.P., Garzione, C.N., Copeland, P., and Upreti, B.N., 2001. Stratigraphy, structure, and tectonic evolution of the Himalayan fold-thrust belt in western Nepal. Tectonics 20, 487-509.

Dyksterhius, S., Albert, R.A., and Muller, R.D., 2005. Finite element modeling of the contemporary and paleo-intraplate stress using ABAQUS™. Computer & Geosciences 31, 297-307.

England, P. and Houseman, G., 1985. Role of lithospheric strength heterogeneities in the tectonics of Tibet and neighbouring regions. Nature 315, 297-301.

England, P. and Houseman, G., 1986. Finite strain calculation of continental deformation, 2, comparision with the India-Asia collison zone. Journal of Geophysical Research 91, 366-36764

England, P., and Molnar, P., 1997. Active deformation of Asia; from kinematics to dynamics. Science 278, 647-650.

Flesch, L.M., Holt, W.E., Haines, A.J., and Shen-Tu, B., 2001. Dynamics of the India-Eurasia Collision zone. Journal of Geophysical Research 106, 16,435-16,460.

Grunthal, G., and Stromeyer, D., 1992. The recent crustal stress field in Central Europe: trajectories and finite element modeling. Journal of Geophysical Research 97, 11,805-11,820.

Harrison, T.M., Copeland, P., Kidd, W.S.F., and Yin, A., 1992. Raising Tibet. Science, 255, 1663-1670.

Hayashi, D. 2007. Unpublished software package, which has been revising every year since 1972.

Hayashi, D., Fujii, Y., Yoneshiro, T., and Kizaki, K., 1984. Observations on the geology of the Karnali region, west Nepal. Journal Nepal Geological Society 4, 29-40.

Homberg, C. Hu, J.C. Angelier, J., Bergerat, F., and Lacombe,O., 1997. Characterization of stress perturbations near majr fault zones: insights from 2-D distinct-element numerical modeling and field studies (Jura Mountains). Journal of Structural Geology 19, 703-718.

Jarosinski, M., Beekman, F., Bada, G., and Cloetingh, S., 2006. Redistribution of recent collison push and ridge push in Central Europe: insights from FEM modeling. Geophysical Journal International 167, 860-880.

Jouanne, F., Mugnier, J.L., Gamond, J.F., Le Fort, P., Pandey, M.R., Bollinger, L., Flouzat, M., and Avouac, J.P., 2004. Current shortening across the Himalayas of Nepal. Geophysical Journal International 157, 1-14.

Kapp, P., and Guynn, J.H., 2004. Indian punch rifts Tibet. Geology 32, 933-996.

Kong, X., and Bird, P., 1996. Neotectonics of Asia:thin-shell finite element models with faults. In Tectonic Evolution of Asia, Yin, A. and Harrison, M. (Eds). Cambridge University Press, 18-34.

Larson, K.M., Burgmann, R. Bilham, R., and Freymuller, J.T., 1999. Kinematics of the India-Asia collision zone from GPS measurements. Journal of Geophysical Research 104, 1077-1093.

Lave, J., and Avouac, J.P., 2000. Active folding of fluvial terraces across the Siwaliks Hills, Himalayas of central Nepal. Journal of Geophysical Research 105, 5735-5770.

Matte, P., Tapponnier, P., Arnaud, N., et al. 1996. Tectonics of Western Tibet, between the Tarim and the Indus. Earth and Planetary Science Letters 142, 311-330.

Meade, B., 2007. Present-day kinematics at the India-Asia Collision zone. Geology 35, 81-84.

Molnar, P., and Tapponnier, P. 1978. Active tectonics of Tibet, Journal of Geophysical Research 83, 5361-5375.

Molnar, P., and Tapponnier, P., 1975. Cenozoic tectonics of Asia: Effects of a continental collision. Science 189, 419 - 426.

Molnar, P., and Chen, W., 1983. Focal depths and fault plane solutions of earthquakes under the Tibetan plateau. Journal of Geophysical Research 88, 1180-1196.

Muller, B., Wehrle,V., Hettel, S., Sperner, B., and Fuchs, K. 2003. A new method for smoothing orientated data and its application to stress data, Geological Society Special Publication 209, 107-126.

Ni, J., and Barazangi, M., 1984. Seismotectonics of the Himalayan collision zone: geometry of the underthrusting Indian plate beneath the Himalaya. Journal of Geophysical Research 89, 1147-1163.

Pandey, M.R., Tandukar, R.P., Avouac, J.P., Lave, J., and Massot, P., 1995. Interseismic strain accumulation on the Himalayan crustal ramp (Nepal). Geophysical Research Letters 22, 751-754.

Pascal, C., and Gabrielsen, R.H., 2001. Numerical modeling of Cenozoic stress patterns in the mid-Norwegian margin and the northern North Sea. Tectonics 20, 585-599.

Patriat, P., and Achache, J., 1984. India-Asia collision chronology and its implicationsfor crustal shortening and driving mechanisms of plates. Nature 311, 615-621.

Petit, C. and Fournier, M., 2005. Present-day velocity and stress fields of the Amurian Plate from thin-shell finite element modeling. Geophysical Journal International 160, 357-369.

Powell, C. McA, and Conaghan, P.J., 1973. Plate tectonics and the Himalayas. Earth and Planetary Science Letters 20, 1-12.

Reinecker, J., Heidbach, O., Tingay, M., Sperner, B., and Muller, B., 2005. The 2005 release of the World Stress Map.

Replumaz, A., and Tapponier, P., 2003. Reconstruction of the deformed collision zone Between Asia by backward motion of lithospheric blocks. Journal of Geophysical Research 108, doi:10.1029/2001JB000661.

Reynolds, S.D., Coblentz, D.D., and Hillis, R.R., 2002. Tectonic forces controlling the regional intraplate stress field in continental Australia: Results from new finite element modeling. Journal of Geophysical Research 107, doi: 10.1029/2001JB000408.

Rothery, D.A., and Drury, S.A., 1984. The neotectonics of the Tibetan Plateau. Tectonics 3, 19-26.

Schelling, D., and Arita, K., 1991. Thrust tectonics, crustal shortening and the structure of the far eastern Nepal Himalaya. Tectonics, 10, 851-862.

Seeber, L. Armbuster, J.G., and Quittmeyer, R.C. 1981. Seismicity and continental

subduction in the Himalayan arc. In: H.K. Gupta and F. Delany (Editors) Zagros, Hindu Kush, Himalaya Geodynamic evolution. American Geophysical Union, Geodynamics Series 3, 215-242.

Shen, F., Royden, L.H., and Burchfiel, C., 2001. Large-scale crustal deformation of the Tibetan Plateau. Journal of Geophysical Research 106, 6,793-6,816.

Soofi, M.A., and King, S.D., 2002. Oblique convergence between India and Eurasia. Journal of Geophysical Research 107, doi: 10.1029/2001JB000636.

Tapponnier, P., Zhiqin, X., Roger, F., Meyer, B., Arnaud, N., Wittlinger, G., and Jingsui, Y., 2001. Oblique stepwise rise and growth of the Tibet Plateau, Science, 294, 1671 - 1677.

Thatcher, W., 2007. Microplate model for the present-day deformation of Tibet. Journal of Geophysical Research 112, doi:10.1029/2005JB004244.

Upreti, B. N., and Le Fort, P., 1999. Lesser Himalayan crystalline nappes of Nepal: problem of their origin. In: Macfarlane, A., Quade, J., Sorkhabi , R., (Eds.), Geological Society of America Special Paper 328, 225-238.

Wang, Q., Pei-Zhen Zhang, P., Freymueller, J.T. Bilham, R., Larson, K.M., Lai, X., You, X., Niu, Z., Wu, J., Li, Y., Liu, J., Yang, Z., and Chen, Q., 2001. Present-day crustal deformation in China constrained by Global Positioning System measurements. Science 294, 574-577.

Yin, A., 2000. Mode of Cenozoic east-west extension in Tibet suggesting a common origin of rifts in Asia during the Indo-Asia collision. Journal of Geophysical Research 105, 21,745 - 21,759.

Yin, A., Kapp, P., Murphy, M., Manning, C.E., Harrison, T.M., Ding, L., Deng, X., and Wu, C., 1999. Evidence for significant late Neogene east-west extension in north Tibet. Geology 27, 787-790.

Zhao, W., Nelson, K.D., Project INDEPTH Team, 1993. Deep seismic reflection evidence for continental underthrusting beneath southern Tibet. Nature 366, 557-559.

Zhonghuai, X. Suyun, W., Yurui, H., and Ajia, G., 1992. Tectonic stress field of China inferred from a large number of small earthquakes. Journal of Geophysical Research 97, 11,867-11,877.

Zoback, M.L., 1992. First- and second-order patterns of stress in the lithosphere: the World Stress Map Project, Journal of Geophysical Research 97, 11,703-11,728.

Zoback, M.L., Zoback, M.D., Adams, J., Assumpcção, M., Bell, S., Bergman, E.A., Blumling, P., Brereton, N.R., Denham, D., Ding, J., Fuchs, K., Gay, N., Gregersen, S., Gupta, H.K., Gvishiani, A., Jacob, K., Klein, R., Knoll, P., Magee, M., Mercier, J.L., Muller, B.C., Paquin, C., Rajendran, K., Stephansson, O., Suarez, G., Suter, M., Udias, A., Xu, Z.H., and Zhizin, M. 1989. Global patterns of tectonic stress. Nature 341, 291-298.